Short-range end resection requires ATAD5-mediated PCNA unloading for faithful homologous recombination

Su Hyung Park[1,2,†], **Namwoo Kim**[1,3,†], **Nalae Kang**[1], **Eunjin Ryu**[1,3], **Eun A. Lee**[1], **Jae Sun Ra**[1], **Anton Gartner**[1,3], **Sukhyun Kang** [1], **Kyungjae Myung** [1,2] and **Kyoo-young Lee** [1,4,*]

[1]Center for Genomic Integrity, Institute for Basic Science, Ulsan 44919, Korea, [2]Department of Biomedical Engineering, College of Information-Bio Convergence Engineering, Ulsan National Institute of Science and Technology, Ulsan 44919, Korea, [3]Department of Biological Sciences, College of Information-Bio Convergence Engineering, Ulsan National Institute of Science and Technology, Ulsan 44919, Korea and [4]Department of Biochemistry, College of Medicine, Hallym University, Chuncheon 24252, Korea

ABSTRACT

Homologous recombination (HR) requires bidirectional end resection initiated by a nick formed close to a DNA double-strand break (DSB), dysregulation favoring error-prone DNA end-joining pathways. Here we investigate the role of the ATAD5, a PCNA unloading protein, in short-range end resection, long-range resection not being affected by ATAD5 deficiency. Rapid PCNA loading onto DNA at DSB sites depends on the RFC PCNA loader complex and MRE11-RAD50-NBS1 nuclease complexes bound to CtIP. Based on our cytological analyses and on an *in vitro* system for short-range end resection, we propose that PCNA unloading by ATAD5 is required for the completion of short-range resection. Hampering PCNA unloading also leads to failure to remove the KU70/80 complex from the termini of DSBs hindering DNA repair synthesis and the completion of HR. In line with this model, ATAD5-depleted cells are defective for HR, show increased sensitivity to camptothecin, a drug forming protein-DNA adducts, and an augmented dependency on end-joining pathways. Our study highlights the importance of PCNA regulation at DSB for proper end resection and HR.

GRAPHICAL ABSTRACT
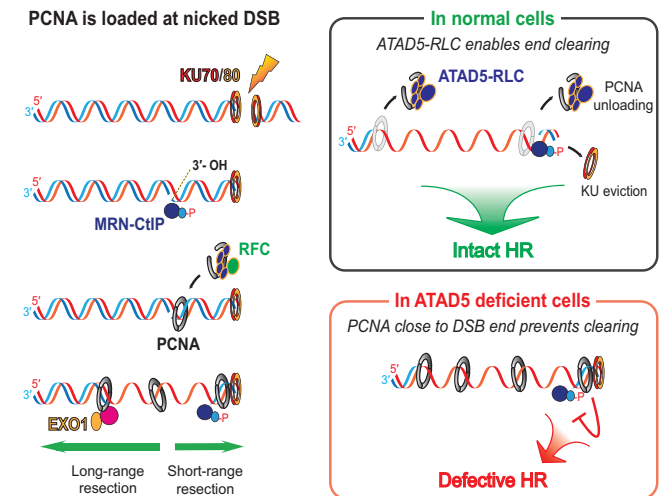
INTRODUCTION

DNA double-strand breaks (DSBs) are one of the most harmful DNA lesions. DSBs are mainly repaired by canonical non-homologous end-joining (c-NHEJ) and HR. The KU70/80-dependent c-NHEJ acts throughout the cell cycle and is potentially error prone. HR is largely error free, generally acts during S and G2 phases, and requires a sister chromatid as a repair template. DSBs can also be mended by DNA polymerase theta (POLθ) mediated end-joining (TMEJ), the Ku protein-independent non-canonical end-joining, and by single-strand annealing (SSA). Both pathways lead to the loss of genetic information, microhomology being used to join DSBs during TMEJ while long repeat sequences are used by SSA (1).

*To whom correspondence should be addressed. Tel: +82 33 248 2543; Email: klee2910@ibs.re.kr
†The authors wish it to be known that, in their opinion, the first two authors should be regarded as Joint First Authors.

HR, TMEJ and SSA all require DNA end resection (1–4), which is initiated by an endonucleolytic nick close to the DSB by the MRE11–RAD50–NBS1 (MRN)-complex bound to CtIP. End resection then proceeds bidirectionally. Short-range resection towards the DSB mediated by the MRN complex produces a short 3′-hydroxyl (3′-OH)-ended single-strand DNA (ssDNA) and displaces KU70/80 heterodimers tightly bound to DSB ends, hindering c-NHEJ and, in particular, being required for HR (5,6). Concomitant long-range resection in the opposite direction catalyzed by EXO1 and the DNA2/BLM complex results into a long 3′-OH ssDNA, which is first coated by replication protein A (RPA), before being replaced by the RAD51 recombinase. RAD51/ssDNA nuclear filaments facilitate homology search and strand invasion into the template DNA, the invading strand being extended by DNA repair synthesis (7).

PCNA plays a critical role as a processivity factor for DNA polymerases and as a binding platform for multiple proteins involved in DNA replication and repair (8,9). PCNA homotrimers are loaded onto DNA at ssDNA/double-strand DNA (dsDNA) junctions at the 3′-OH end, primarily by the pentameric replication factor C (RFC) complex composed of RFC1-5 (10,11). When DNA synthesis is completed, PCNA is unloaded by the ATAD5-RFC-like-complex (RLC) encompassing ATAD5 and RFC2-5 (12–14).

The RFC complex, PCNA and ATAD5-RLC were reported to play a role in HR (15–18). In addition to their roles in DNA repair synthesis during HR (19–21), several reports suggested additional roles of PCNA in regulating HR right after DSB formation: The RFC complex and PCNA rapidly associate with DSBs (22). Elg1, the budding yeast ATAD5 homologue, associates with DSBs sites independent of Rad52, a key mediator of RAD51 loading (18). In addition, PCNA has been suggested to promote EXO1-mediated long-range resection (23). Those findings prompted us to ask the followed questions: i) which DNA structures pertinent to DSB processing are associated with PCNA? ii) does PCNA loading require the RFC complex? iii) and does PCNA need to be unloaded by ATAD5-RFC-like complex (RLC)?, and if so iv) does excessive PCNA lead to the dysregulation of end resection, resulting in defective DNA repair?.

ATAD5 (Elg1) is important for the maintenance of genomic stability (24), and this is underscored by a high level of tumors in haploinsufficient *Atad5* mice, and frequent somatic mutations in *ATAD5* in human tumors (17,25–27). Accumulating data suggests that PCNA that fails to be unloaded and remains on DNA might be a primary cause of defects during DNA replication and DNA repair (13,24,28–33). Here, we investigate PCNA loading during short-range resection, and the requirement for ATAD5 dependent PCNA unloading for faithful HR.

MATERIALS AND METHODS

Cell lines and cell culture

HeLa, U2OS, U2OS-ATAD5^{AID} (30), $POLQ^{+/+}$ and $POLQ^{-/-}$ DR-U2OS (34) (kindly provided by Dr Kei-ichi Taketa), U2OS-DR-GFP, U2OS-EJ5-GFP, U2OS-EJ2-GFP, U2OS-SA-GFP cells (kindly provided by Dr Jeremy Stark), U2OS 2–6–5 cells stably expressing destabilization domain (DD)-estrogen receptor (ER)-FokI endonuclease-mCherry-Lac repressor (LacR) fusion protein (DD-ER-FokI-mCherry-LacR) (kindly provided by Dr Roger Greenberg), HeLa-PCNA^{GFP}, $ATAD5^{+/+}$ and $ATAD5^{-/-}$ HEK293AD and U2OS cells (35) were cultured in Dulbecco's modified Eagle medium containing 10% fetal bovine serum (FBS; GE Healthcare), 100 U/ml penicillin G (Life Technologies) and 100 μg/ml streptomycin (Life Technologies) in a humidified atmosphere of 5% CO_2 at 37°C.

Small interfering RNAs (siRNAs), and transfection

The following synthetic duplex siRNAs were purchased: ATAD5 3′ UTR (5′-GUAUAUUUCUCGAUGUACA-3′) (13), PARP1 (5′-CUUCGUUAGAAUGUCUGCCUU-3′), RFC1 (#SN-5981-1), MRE11 (#SN-4361-1), XRCC1 (#SN7515-1), BRCA1 (5′-CAGCAGUUUAUUACUCAC UAA-3′), BRCA2 (5′-UUGGAGGAAUAUCGUAGGUA A-3′), and control siRNA (#SN-1002) (Bioneer); CtIP (L-011376–00) (Horizon Dharmacon); KU80 (#SI02663766) (QIAGEN). Transfection of cells with 20 nM siRNAs was performed using RNAiMAX (Thermo Fisher Scientific) according to the manufacturer's instructions. Transfection of plasmid DNA was performed using X-tremeGENE™ HP (Roche) or Lipofectamine 3000 (Thermo Fisher Scientific). Cells were analyzed 48 h after transfection, unless otherwise specified.

Reagents and antibodies

The following chemicals were used in this study: camptothecin (C9911), etoposide (E1383), bleomycin (B1141000), B02 (SML-0364), PFM39 (SML-1839) and 4-hydroxytamoxifen (tamoxifen) (H7904) (Sigma-Aldrich); indole-3-acetic acid (IAA, auxin) (87-51-4) (Millipore); MIRIN (S8096) (Selleckchem); Shiled-1 (632189) (TAKARA). PFM01 and PFM03 were kindly provided by Dr John Tainer (MD Anderson Cancer Center). The following antibodies were used: anti-PCNA (PC10, sc-56), anti-RFC1 (B-5), anti-RFC4 (H-183, sc-20996) and anti-RAD54 (F-11, sc-374598) (Santa Cruz Biotechnology); anti-RPA2 (A300-244A) and anti-KU80 (A302-627A) (Bethyl Laboratories); anti-KU80 (MA5-12933) (Invitrogen); anti-PCNA (ab18197), anti-β tubulin (ab-15568) and anti-GAPDH (ab181603) (Abcam); anti-FLAG (F7425) and anti-Actin (A3853) (Sigma-Aldrich); anti-RAD51 (Cell Signaling Technology); anti-histone H3 and anti-β actin (BA3R) (Thermo Fisher Scientific); anti-MRE11 antibody (NB100-142) (Novus Biologicals); anti-Myc (4A6) and anti-γH2AX (05–636) (Merck Millipore); anti-BrdU (347580) (BD Biosciences) antibodies. The anti-human ATAD5 antibody was raised in rabbits against an N-terminal fragment (1–297 aa) (36).

355-nm UV-laser microirradiation and X-ray irradiation

For the microirradiation, HeLa-PCNA^{GFP} cells plated on LabTek™ Chambered Coverglasses (Thermo Fisher Scientific) were pre-sensitized with 10 μM BrdU for 24 h. UV

microirradiation was then applied to cells using a Diode 355-nm laser (100% power) projected through a C-Apochromat 40×/1.2 W Korr FCS M27 objective, via a bleaching module (5 iterations) on a Zeiss LSM880 confocal microscope (Carl Zeiss, Oberkochen, Germany) platform. After irradiation, live cell images were obtained with a time-lapse setting of ZEN 2.6 (blue edition) (Carl Zeiss) software. The signal intensity of GFP signals on the microirradiated strip was quantified using ZEN 2.6 software. Relative intensities, adjusted to the baseline of 100 were displayed. For X-ray irradiation, cells plated on LabTek™ chamber slides (Thermo Fisher Scientific) or cover slips (Marienfeld) were irradiated using the RS 2000 X-ray irradiator (RAD SOURCE) following manufacturer's protocol.

FokI-induced DSB generation

U2OS-LacO reporter cells stably expressing DD-ER-FokI-mCherry-LacR were transfected with siRNA or cDNA and, after 48 h, treated with 1 μM tamoxifen (binds to ER and induces nuclear transport of proteins fused to ER) and 1 μM Shield1 (stabilizes proteins tagged with a DD domain) for 4 h to induce DSBs, and fixed. For chemical inhibition of RAD51, 20 μM B02 were used for treatment together with tamoxifen. For chemical inhibition of MRE11, cells were exposed to 500 μM MIRIN and 200 μM PFM39 for 1 h before DSB induction and maintained throughout incubation.

Immunostaining

Cells plated on LabTek™ chamber slides (Thermo Fisher Scientific) were fixed and stained as described previously (13) with slight modifications. Briefly, the cells were pre-extracted with cytoskeleton (CSK) buffer (10 mM PIPES, 100 mM NaCl, 300 mM sucrose, 3 mM $MgCl_2$, 1 mM EGTA and 0.5% Triton X-100™) for 10 min on ice and fixed with 4% paraformaldehyde (PFA) for 20 min at room temperature. For denatured BrdU staining, cells were treated with 2 N HCl for 30 min after fixation. For RAD54 immunostaining, cells were first fixed with 4% PFA and treated with the CSK buffer. After washing with phosphate-buffered saline (PBS) and incubating in blocking buffer (10% FBS in PBS) for 30 min, cells were incubated with the indicated antibodies diluted in blocking buffer at 4°C overnight. After three washes with 0.05% Triton X-100 in PBS, Alexa Fluor-conjugated secondary antibodies (Thermo Fisher Scientific) were added and incubated for 30 min. After washing, cells were mounted using ProLong Gold antifade reagent with DAPI (Vector Laboratories, Burlingame). For KU80 immunostaining, we followed a previously reported protocol (37). Confocal images were acquired using a Zeiss LSM880 confocal microscope with a 40×/1.2 objective. Image acquisition and analysis were performed with ZEN 2.6 (blue edition) software. For nuclear intensity analysis, nuclei were first masked, and the mean intensity within the masked regions was measured.

Cell cycle specific IR-induced DNA repair synthesis

IR-induced DNA repair synthesis at G2 cells was measured as described previously (19) with slight modifica-

tions. Briefly, Cells were treated with 10 μM 5-bromo-2′-deoxyuridine (BrdU) for 1 h, X-ray irradiated, and incubated with 10 μM 5-ethynyl-2′-deoxyuridine (EdU) for 8 h. Cells were then fixed with 4% PFA for 20 min, extracted with CSK buffer, and treated with 2 N HCl for 30 min for BrdU immunostaining. For EdU detection, cells were then processed using the Click-iT EdU Imaging kit (Thermo Fisher Scientific) according to the manufacturer's instructions. BrdU-positive cells were identified as S-phase cells, while the BrdU-negative cells were categorized as either G1 or G2 based on their DNA content (Supplementary Figure 6A).

Proximity ligation assay (PLA)

For the MRE11-PCNA PLA, cells were incubated in CSK buffer (10 mM PIPES, 100 mM NaCl, 300 mM sucrose, 3 mM $MgCl_2$, 1 mM EGTA and 0.5% Triton X-100™) for 10 min at 4°C, fixed with 4% PFA for 20 min at room temperature, blocked with 10% fetal bovine serum in PBS for 1 h. After blocking, cells were incubated with primary antibody overnight at 4°C with 1:250 rabbit anti-MRE11 antibody (NB100-142) with 1:250 mouse anti-PCNA antibody (PC-10). The next day, after washing with 1× PBS twice, cells were incubated with pre-mixed Duolink PLA plus and minus probes for 1 h at 37°C in a humidity chamber. The subsequent steps in proximal ligation assay were carried out using the Duolink® PLA Fluorescence kit (Sigma) according to the manufacturer's instructions. Slides were then stained with DAPI and imaged on a Zeiss LSM880 confocal microscope.

I-SceI-induced DSBR assay

I-SceI-induced DSBR assay was performed using U2OS-based reporter cell lines (DR-GFP for HR, EJ5-GFP for canonical NHEJ, EJ2-GFP for alternative EJ including TMEJ, and SA-GFP for single-strand annealing) as described previously (38). Briefly, reporter cells were plated on a 12-well plate at 1×10^5 cells/well. The following day, each cell line was transfected with 20 nM siRNA. After 24 h, cells were transfected again with 0.5 μg of either pCAGGS-I-SceI (called pCBASce) or empty pCAGGS-BSKX vector, and 0.1 μg of dsRed expression vector. Two days after I-SceI transfection, cells were analyzed using a BD FACS-Verse flow cytometer with BD FACSuite software. Repair efficiency was calculated by dividing the percentage of GFP-positive cells to the percentage of dsRed-positive cells. Data analysis was done using Flowjo software.

RPA retention assay using flow cytometry

IR-induced chromatin RPA2 was measured as described previously (39) with slight modifications. Cells were irradiated and incubated for 2 h. 4 μM aphidicolin was added immediately after IR to block S to G2 progression. After incubation, cells were trypsinized, washed with PBS and permeabilized with 100 μl of 0.2% Triton X-100 in PBS for 10 min on ice. Cells were then added with 1 ml of 1 × perm/wash buffer (0.5% Tween 20 and 0.5% bovine serum albumin in PBS), centrifuged and fixed with 3% PFA–2% sucrose in

PBS for 15 min at room temperature. After washing with 1ml of 1 × perm/wash buffer, cells were incubated with 50 μl of mouse anti-RPA2 antibody (1:100, Calbiochem, NA19L) in 1 × perm/wash buffer for 45 min each at 37°C. After washing with 1 ml of 1 × perm/wash buffer, cells were incubated with 50 μl Alex Flor488-conjugated anti-mouse secondary antibody (1:500) in 1 × perm/wash buffer for 45 min each at 37°C. After washing with 1ml of 1 × perm/wash buffer, cells were resuspended in 10 μg/ml propidium iodide (Sigma-Aldrich) and 100 μg/ml RNase A (RBC) and analyzed using a BD FACSVerse flow cytometer with BD FACSuite software. G2 cells were identified on the basis of their DNA content assessed by propidium iodide staining. Data analysis was done using FlowJo software.

Cell survival assay

Cells were seeded in 96-well culture plates. After 24 h, cells were treated with drugs for indicated period and processed using the CellTiter-Glo® 2.0 Assay kit (Promega) according to the manufacturer's instructions. In brief, cells were lysed with CellTiter-Glo® reagent and the luminescence signal was read using a plate reader. Percent cell survival was normalized to that of control cells. For clonogenic survival assays, control wild type cells and U2OS-ATAD5^{AID} cells were seeded onto 60 mm plates at a density of 5×10^2 cells/60 mm. Cells were pre-treated with auxin for 24 h, treated with Olaparib for 96 h and washed with PBS followed by addition of fresh medium and incubation for 14 days. Cells were then washed with PBS and stained with 2% methylene blue in 70% EtOH for 10 min.

Analysis of metaphase chromosomes

Cells were incubated for 6 h with 0.2 μg/ml colcemid and then metaphase cells were harvested by trypsinization. The cells were then swollen in 75 mM KCl for 15 min at 37°C and fixed with methanol:acetic acid (3:1) twice. Cells were dropped onto glass microscope slides and stained with 5% Giemsa stain. Images were acquired using a fluorescence microscope (BX53; Olympus). At least 35 metaphase cells were taken randomly from each condition.

Cell cycle analysis

Cells were washed with PBS, fixed with 70% ethanol for 1 h, and then incubated with 0.1 mg/ml RNase A at 37°C for 1 h. DNA was stained with 0.05 mg/ml propidium iodide. Flow cytometry was performed on a FACSVerse™ flow cytometer using BD FACSuite™ software (BD Biosciences). Data analysis was performed using FlowJo software.

Sequence analysis of repair product in DR-GFP construct

U2OS-DR-GFP reporter cells seeded onto a 100 mm dish were transfected with 20 nM siRNA. After 24 h, cells were co-transfected again with 5 μg pCAGGS-I-SceI and 1 μg dsRed expression vector. Two days after I-SceI transfection, dsRed-positive cells were sorted using a BD FACSAria fusion. Genomic DNA was isolated from the sorted cells, PCR- amplified using 2 μg of genomic DNA

and the primers P1 (5′-CTGCTAACCATGTTCATGCC-3′) and P2 (5′- AAGTCGTGCTGCTTCATGTG-3′), purified, and digested with 10 U of I-SceI (New England Biolabs) overnight, as previously described (38). The undigested PCR product was gel purified and cloned into pGEM-T Easy Vector (Promega) and sequence was analyzed.

Protein extraction, immunoprecipitation, and immunoblot analysis

Whole cell extracts were isolated by incubating cell pellets with RIPA buffer (50 mM Tris–HCl, pH 8.0, 150 mM NaCl, 5 mM EDTA, 1% Triton X-100™, 0.1% sodium dodecyl sulfate, 0.5% sodium deoxycholate, 0.1 M phenylmethylsulfonyl fluoride and 1× cOmplete Protease Inhibitor Cocktail [Roche]) with Benzonase nuclease for 45 min on ice followed by sonication and centrifugation. Isolation of a Triton X-100–insoluble fraction (chromatin-bound fraction) was performed as previously described (36) with slight modifications. In brief, the soluble fraction was removed by incubating cells in buffer A (100 mM NaCl, 300 mM sucrose, 3 mM MgCl₂, 10 mM PIPES, pH 6.8, 1 mM EGTA, 0.2% Triton X-100™, phosphatase inhibitors and protease inhibitors [Roche]) for 5 min on ice followed by centrifugation. Then, the detergent-insoluble fraction was isolated by resuspending the pellet in RIPA buffer containing Benzonase nuclease, followed by sonication and centrifugation. For immunoprecipitation, proteins were incubated with specific antibodies. Then, the complex recognized by antibodies was precipitated with protein G-Sepharose beads. For immunoblot analysis, proteins were separated by SDS-PAGE and transferred to a nitrocellulose membrane. Blocking of the membranes and blotting with primary antibodies were performed in Tris-buffered saline containing 0.1% Tween® 20 supplemented with 5% skim milk powder. Proteins were visualized using secondary horseradish peroxidase-conjugated antibodies (Enzo Life Sciences) and enhanced chemiluminescence reagent (Thermo Fisher Scientific). Signals were detected using an automated ChemiDoc™ imaging system (Bio-Rad Laboratories).

Protein purification

Human MR complex were expressed in sf9 insect cells (Thermo Fisher Scientific) with the Bac-to-Bac Baculovirus expression system (Thermo Fisher Scientific). MRE11 and RAD50 cDNAs were cloned into the MultiBac Baculovirus/Insect Cell Expression Vector, pFL (pFL-2xStrep-MRE11_RAD50-HA-6xHis) to co-express two proteins in insect cells. The MR complex was purified as described previously (40) with slight modification. Insect cells expressing MR complex were lysed and sonicated in 0.5 M KCl-buffer S (50 mM KH₂PO₄ pH 7.5, 10% glycerol, 1 mM DTT with 1× cOmplete Protease Inhibitor Cocktail [Roche]). The lysates were cleared by ultracentrifugation (36 000×g, 60 min) and applied to Strep-Tactin Sepharose resin (GE Healthcare), washed and eluted with 0.05 M KCl-buffer S containing 2.5 mM d-Desthiobiotin. The eluate was then loaded onto a Hi-Trap SP column (GE Healthcare) pre-equilibrated with 0.1 M KCl-buffer SP

(75 mM Tris–HCl pH 8.0, 10% Glycerol, 1 mM DTT), washed, and sequentially eluted with 0.2–0.6 M KCl-buffer SP. Human PCNA, human RFC1 (△N554)-RFC, human ATAD5 (△N692)-RLC and human ATAD5 (△N692, E1173K)-RLC were purified as described previously ([12]). Purified proteins were analyzed by SDS-PAGE and Coomassie blue staining. Aliquoted proteins were frozen and stored at −80°C.

Preparation of dsDNA substrate for resection assay

The following synthetic oligomers were purchased from Bioneer (Daejeon, Korea): Oligomer 1 (5′-AACGTCAT AGACGATTACATTGCTAGGACATCGATTCCAG TCAGTTTGCCCACGTTG∗A∗C∗C∗A∗A-3′; * indicates phosphorothioate bond), Oligomer 2 (5′-GATGTCCTA GCAATGTAATCGTCTATGACGTTA-Biotin-3′), and Oligomer 3 (5′-[Cy-5]T[Biotin-dT]GGTCAACGTGGG CAAACTGACTGGAATC-3′). To prepare Cy-5 labeled dsDNA substrates, 10uM of oligomers were annealed in 1x annealing buffer (10 mM Tris–HCl pH 7.4, 50 mM NaCl without EDTA) by cooling from 95°C to 15°C at a rate of −5°C/3 min.

In vitro resection assay

MR resection assays were performed as described previously ([40]). Protein was diluted in buffer H (25 mM HEPES pH 7.5, 1 mM EDTA, 1 mM EGTA, 10% glycerol, 1 mM DTT, 1 mM ATP) containing 5 mM magnesium acetate (MgOAc) with specific salt concentration (100 mM potassium acetate [KOAc] for RFC and PCNA and 300 mM KCl for MR and ATAD5-RLC). For MR reactions, 1 nM Cy-5 labeled dsDNA substrates were pre-incubated with 50 nM streptavidin, and 1 mM ATP in $1\times$ MR reaction buffer (25 mM MOPS pH 7.0, 2 mM DTT, 8% Glycerol, 0.2 mg/ml BSA, 5 mM $MnCl_2$ and 5 mM $MgCl_2$) in room temperature for 10 min (the dsDNA-streptavidin premix). 150 nM MR was then directly added to the dsDNA-streptavidin premix with salt concentration normalized by KCl, and the reaction mixture was incubated at 37°C for 30 min. For loading PCNA onto dsDNA substrates before the MR reaction, 0.56 nM RFC1 (△N554)-RFC and 112 nM PCNA were added to the dsDNA-streptavidin premix with salt concentration normalized with KOAc, and incubated at 37°C for 30 min before MR addition. To add PCNA unloading reaction, 25 nM ATAD5 (△N692)-RLC or ATAD5 (△N692, E1173K)-RLC were added with salt concentration normalized with KCl at 15 min after incubation of dsDNA-streptavidin premix with RFC and PCNA, and incubated at 37°C for 15 min before MR addition. MR reaction was stopped with 0.2% SDS and 10 mM EDTA, and protein was removed by incubating with 10 μg proteinase K at 37°C for 2 h. DNA was isolated by chloroform extraction, and the isolated DNA was lyophilized overnight, dissolved in formamide, boiled at 95°C for 5 min, loaded on denaturing polyacrylamide gel containing 1x TBE, 15% acrylamide and 7 M urea, and separated at 200V for 3 h. Cy-5 labeled DNA in the gel was detected by Amersham Typhoon Biomolecular Imager (Cytiva).

To confirm that the dsDNA substrate can load PCNA, annealed DNA substrates were attached to streptavidin-coated magnetic beads (Dynabeads M-280 [Invitrogen]), unbound DNA substrates were discarded, and the bound substrates was diluted in buffer H containing 300 mM KOAc and 0.01% NP40, and PCNA loading reactions were performed using 5 nM DNA substrate attached to bead under the same conditions as in the *in vitro* resection assay. After the reaction, beads were washed with 0.3 M KCl- and 0.5 M KCl-buffer H, and DNA was digested by 125 U Benzonase at 37°C for 10 min. The eluted protein was then analyzed by immunoblot analysis.

Statistical analysis

Prism 8 (GraphPad Software) was used to generate graphs and analyze data. For all data, two-tailed unpaired Student's t-tests or ANOVA, along with a post-hoc Tukey test were used; ****$P < 0.001$, *** $P < 0.005$, ** $P < 0.01$, * $P < 0.05$ and ns: not significant. Statistical parameters are described in the figures.

RESULTS

PCNA is rapidly loaded on DNA at DSB sites by RFC and later unloaded by ATAD5-RLC

We first investigated whether ATAD5 is localized at DSB sites. Both endogenous ATAD5 and mNeonGreen-ATAD5 localized at FokI-induced DSBs (Figure 1A), upon generating localized DSBs at an array of lac operators by tethering the FokI endonuclease fused to mCherry-LacR ([41]). We found that RFC1 depletion reduced the localization of mNeonGreen-ATAD5 at FokI-induced DSBs (Figure 1B), suggesting a dependence on PCNA loaded by the RFC complex. PCNA loading and unloading occur as part of the DNA repair synthesis that occurs when the invading strand is extended ([19–21]). To determine whether ATAD5 is also recruited before DNA repair synthesis, we blocked strand invasion by treating cells with the B02 RAD51 recombinase inhibitor, known to abolish RAD51 filament formation and DNA repair synthesis (Supplementary Figure 1A) ([42]). We found that mNeonGreen-ATAD5 location at FokI-induced DSBs was not reduced upon B02 treatment, irrespective of RFC1 status (Figure 1B). Similar to ATAD5, PCNA was rapidly recruited to the microirradiated strips, recruitment being reduced by RFC1 depletion (Figure 1C and D). PCNA also co-localized at FokI-induced DSBs, irrespective of B02 treatment (Supplementary Figure 1B). Consistently, depletion of BRCA2, which is a key HR factor required for RAD51 loading onto ssDNA and subsequent strand invasion ([1,3]), did not affect PCNA signal on laser microirradiated strips (Figure 1E and F). Taken together, our results suggest that the rapid PCNA recruitment to DSBs is largely dependent on RFC-mediated loading and that this may occur independent of DNA repair synthesis which requires strand invasion.

In line with the PCNA unloading activity of ATAD5, PCNA hyper accumulated and remained longer on microirradiated strips in ATAD5-depleted HeLa cells (Figure 1G-I) and U2OS cells (Supplementary Figure 1C and D), as
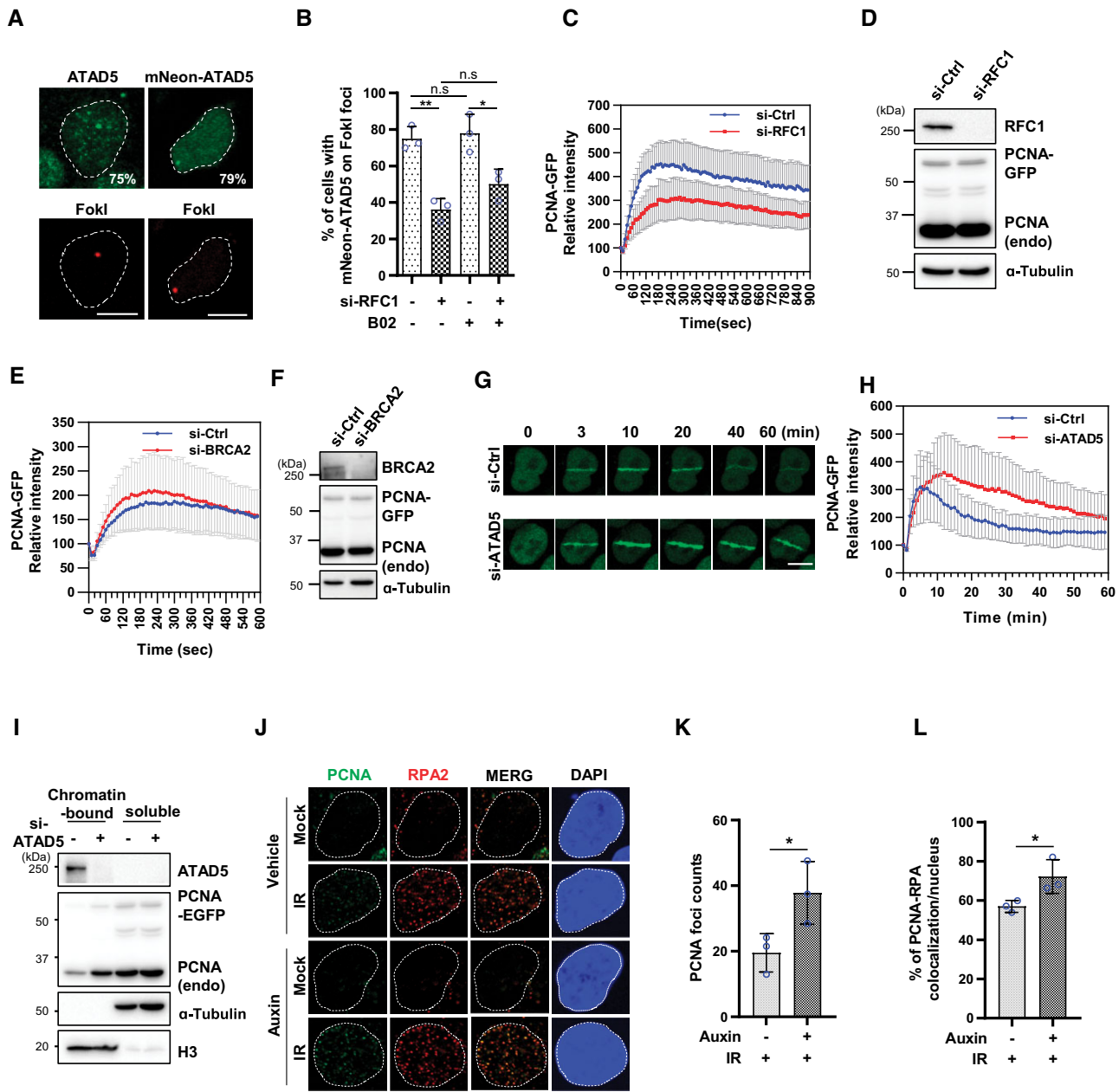
Figure 1. PCNA is rapidly recruited to DSBs, and recruitment requires RFC1 but not DNA repair synthesis. (**A**) U2OS-LacO reporter cells stably expressing DD-ER-FokI-mCherry-LacR were treated with tamoxifen and Shield1 for 4 h to induce DSBs. Endogenous ATAD5 visualized by immunostaining (left panels) and mNeonGreen-ATAD5 imaged after transfection 48 h before DSB induction (right panels). The incidence of costaining between FokI (red) and ATAD5 is indicated in the upper panels. (**B**) U2OS-LacO reporter cells stably expressing ER-DD-mCherry-LacR-FokI were co-transfected with mNeonGreen-ATAD5 cDNA and either control or *RFC1* siRNA, and, after 48 h, DSB was induced. Cells were treated with B02 together with tamoxifen and Shield1. Error bars represent SD. Statistical analysis: One-way ANOVA. (**C–I**) HeLa cells stably expressing PCNA fused with enhanced green fluorescence protein (GFP) (HeLa-PCNA[GFP]) were transfected with *RFC1* siRNA (**C, D**), *BRCA2* siRNA (**E, F**) or *ATAD5* siRNA (**G–I**) and subjected to UV microirradiation (**C, E, G, H**), and whole cell extracts (D, F) or soluble and chromatin-bound protein extracts (**I**) were prepared for immunoblotting. (C, E, H) Relative intensities, adjusted to the baseline of 100 are displayed. Error bars represent SD ($n = 18$ for si-Ctrl; $n = 17$ for si-RFC1 [C], $n = 19$ [E], $n = 10$ [H]). (**G**) Representative images of single cells. (**J–L**) U2OS-ATAD5[AID] cells were treated with auxin, subjected to X-ray treatment (6 Gy), incubated for 30 min and fixed for immunostaining. (**J**) Representative images. (**K, L**) Quantification of PCNA foci (K) and colocalization between PCNA and RPA2 (L). G2 cells were identified based on the PCNA foci pattern and DNA content as determined by DAPI staining. Error bars represent SD. Statistical analysis: two-tailed unpaired Student's *t*-test. (A, G, J) Scale bar 10 μm.

well as in HEK293AD *ATAD5* knockout cells (Supplementary Figure 1E and F). Even when image acquisition time was extended to 4 hours, PCNA was still remained on microirradiated strips in ATAD5-depleted cells (Supplementary Figure 1G and H). Furthermore, ionizing radiation (IR)-induced PCNA foci (monitored in cells residing in the G2 cell cycle stage) were increased upon auxin treatment of U2OS cells carrying AID-tagged ATAD5 (U2OS-ATAD5^{AID}) (30) (Figure 1J and K). Under the same conditions, IR-induced RPA2 foci, representing DSB sites undergoing repair, were not altered (Figure 1J and Supplementary Figure 1I). PCNA foci, some of which were colocalized with RPA2, appeared within 30 min after IR treatment in G2 cells (Figure 1J), the number of PCNA foci and colocalization with RPA2 being increased upon auxin-mediated ATAD5 depletion (Figure 1J and L). Taken together, PCNA is rapidly recruited to DSBs and hyper accumulates upon ATAD5-RLC depletion, consistent with ATAD5-RLC dependent unloading.

PCNA recruitment to DNA damage sites largely depends on MRN-CtIP

Given the RFC1 requirement for PCNA recruitment to DSBs, we speculated that PCNA might be loaded at nicks and/or short single-stranded gaps, generated by MRN-CtIP endo/exonuclease activity close to DSB sites (Figure 2A) (12). Consistent with this hypothesis, the recruitment of PCNA to microirradiated strips was reduced when CtIP or MRE11 were depleted (Figure 2B–E) or when MRE11 endonuclease inhibitors PFM01 or PFM03 were treated (Figure 2F). Conversely, treatment with the MRE11 exonuclease inhibitor PFM39 led to an increase in PCNA signals on the microirradiated strips (Figure 2G), suggesting that continuous PCNA loading occurs in cases of short-range resection defects. Consistent with this, mNeon-ATAD5 localization at FokI-induced DSBs was reduced upon CtIP or MRE11 depletion (Figure 2H and I). Treatment with the MRE11 exonuclease inhibitors mirin or PFM39 also reduced mNeon-ATAD5 localization at FokI-induced DSBs (Figure 2J), suggesting that there is a mechanism to restrict ATAD5-RLC access to PCNA that has not completed its task, as exemplified by the inhibition of premature PCNA unloading by acetylated histones during DNA replication (43).

ATAD5 is important for HR but not for other DSBR pathways

ATAD5-depleted cells were reported to be defective for HR (16,17). Given our finding that PCNA recruitment to DSBs requires MRN-CtIP, and HR, TMEJ and SSA all being known to require end resection (3,4), we examined the effects of ATAD5 depletion on these DSBR pathways, as well as on c-NHEJ, using tailored I-SceI-based reporter assays, scoring for the restoration of GFP expression (Supplementary Figure 2A–D) (38). After I-SceI-induced DSB generation, DR-GFP, SA-GFP, EJ2-GFP and EJ5-GFP DNA recover GFP expression when they are repaired by HR, SSA, alternative EJ including TMEJ and c-NHEJ, respectively. CtIP depletion reduced the frequency of HR, SSA and

TMEJ, but increased the frequency of c-NHEJ (Figure 3A), as reported (44). ATAD5 depletion reduced the frequency of HR as reported (17), while other DSBR pathways including c-NHEJ, TMEJ and SSA remained intact (Figure 3A). Supporting a role for ATAD5 in the HR pathway, the decrease in HR frequency induced by depletion of BRCA1, a key factor for commitment to the HR pathway (1,3), was not further reduced by ATAD5 depletion (Supplementary Figure 3A). In addition, ATAD5-depleted cells were sensitive to the PARP1 inhibitor Olaparib in both acute viability assays and colony survival assays (Figure 3B–D) as previously reported (16,45). This result is in line with the reported requirement of PARP1-mediated repair for the survival of HR-deficient cells (46,47). Taken together, our data underline a HR-specific role of ATAD5 in DSBR.

ATAD5-depleted cells are sensitive to a drug forming protein-DNA adducts

We next examined the sensitivity of ATAD5-depleted cells to various DSB-inducing reagents. *ATAD5*$^{-/-}$ U2OS and HEK293AD cells were not hypersensitive to bleomycin and X-ray treatment, consistent with breaks induced by such treatment being mainly repaired by c-NHEJ (48) (Figure 3E–G, Supplementary Figure 3B and C). In contrast, we observed a mild hypersensitivity to the DNA topoisomerase-1 (TOP-1) inhibitor camptothecin (CPT) in both *ATAD5*$^{-/-}$ cell lines (Figure 3H and Supplementary Figure 3D), with a comparable cell cycle profile independent of the presence of ATAD5 (Supplementary Figure 3E and F). In addition, the number of CPT-induced chromosome breaks and fragmented chromosomes was increased in ATAD5-depleted cells (Figure 3I and J). CPT traps TOP-1 cleavage complexes (49). TOP-1 trapped to single-strand breaks, upon DNA replication results into DSBs reported to be mainly repaired by HR (7). In support of a role for ATAD5 in the HR pathway, the hypersensitivity to CPT induced by BRCA1 depletion was not further exacerbated by ATAD5 depletion (Supplementary Figure 3G and 3H). We reasoned that the mild sensitivity of *ATAD5*$^{-/-}$ cells to CPT is due to the compensatory activity of other DSBR pathways. Consistent with this notion, we found that the depletion of ATAD5 in TMEJ-defective U2OS *POLQ*$^{-/-}$ cells results in hypersensitivity to CPT (Figure 3K and L).

Recruitment of MRN-CtIP and EXO1 to the DSBs and DNA damage checkpoint are intact in ATAD5-depleted cells

We next tried to find the cause of HR defects associated with ATAD5 deficiency. We first investigated whether ATAD5 affects recruitment of nucleases involved in DNA end resection to the DSBs. As a result, we found that recruitment of MRE11, NBS1, CtIP and EXO1 to FokI-induced DSBs or laser microirradiated strip was not affected by ATAD5 depletion (Supplementary Figure 4A–L).

Elg1, the budding yeast ATAD5 homologue, was reported be involved in the DNA damage checkpoint signal (50). Considering known role of ATM and ATR in promoting DNA damage response and HR by phosphorylating several key proteins, including CtIP, MRE11 and NBS1 (51), we investigated whether ATAD5 depletion affects DNA damage checkpoint signal. As a result, we found
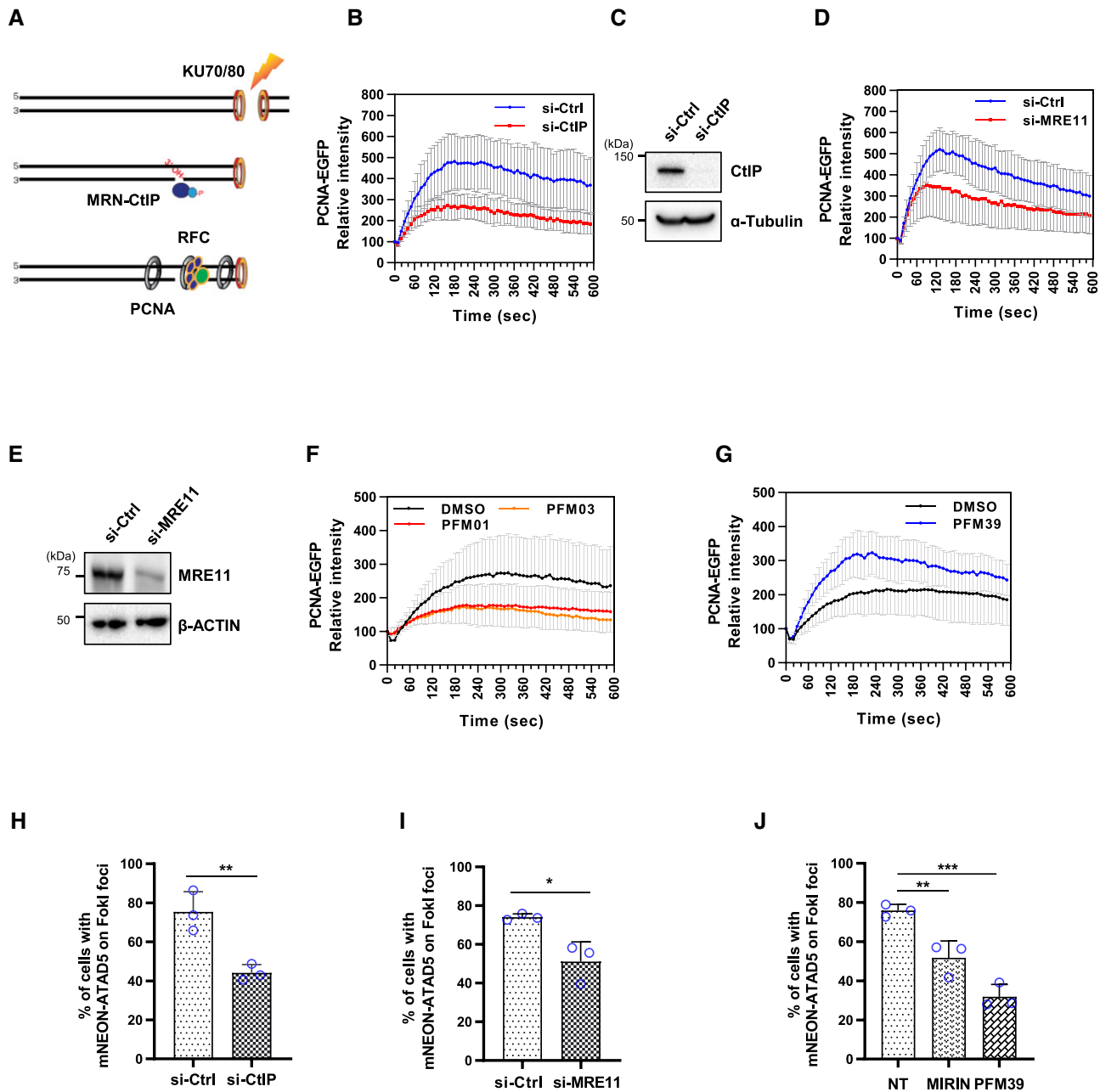
Figure 2. PCNA and ATAD5 are recruited to DSBs, and recruitment requires MRN-CtIP. (**A**) Model of PCNA loading on nicked DNA in proximity to DSBs. (**B–E**) HeLa-PCNA^{GFP} cells were transfected with *CtIP* siRNA (**B, C**) or *MRE11* siRNA (**D, E**) and subjected to UV microirradiation (B, D), and whole cell extracts were subjected to immunoblotting (C, E). (B, D) Relative intensities, adjusted to the baseline of 100 are displayed. Error bars represent SD ($n = 14$ for si-Ctrl; $n = 12$ for si-CtIP [B], $n = 15$ for si-Ctrl; $n = 14$ for si-MRE11 [D]). (F, G) HeLa-PCNA^{GFP} cells were pre-treated with 50 μM PFM01, 50 μM PFM03 (**F**) or 50 μM PFM39 (**G**) for 30 min and subjected to UV microirradiation. Relative intensities, adjusted to the baseline of 100 are displayed. Error bars represent SD ($n = 21$ for DMSO; $n = 17$ for PFM01; $n = 18$ for PFM03 [F], $n = 21$ for DMSO; $n = 16$ for PFM39 [G]). (**H–J**) U2OS-LacO reporter cells stably expressing DD-ER-FokI-mCherry-LacR were co-transfected with mNeonGreen-ATAD5 cDNA and with *CtIP* siRNA (**H**) or *MRE11* siRNA (**I**), or treated with MIRIN and PFM39 for 5 h before fixation (**J**). Error bars represent SD. Statistical analysis: one-way ANOVA.

that IR-induced phosphorylation of CHK1, CHK2 and gamma H2AX was not reduced by ATAD5 depletion (Supplementary Figure 4M).

Long-range resection is intact in ATAD5-depleted cells

Next, we examined the effect of ATAD5 depletion on DNA end resection. The extent of end resection was gauged cy-tologically by first incorporating Bromo-2′-deoxyuridine (BrdU) into DNA, BrdU only being detectable in single-stranded DNA generated by end resection. We found that the intensity of the BrdU signal increased above back-ground upon IR treatment, the signal intensity not being affected by ATAD5 depletion (Supplementary Figure 5A and 5B). In addition, we measured RPA2 loading on re-sected DNA. Gating G2 cells (Supplementary Figure 5C,
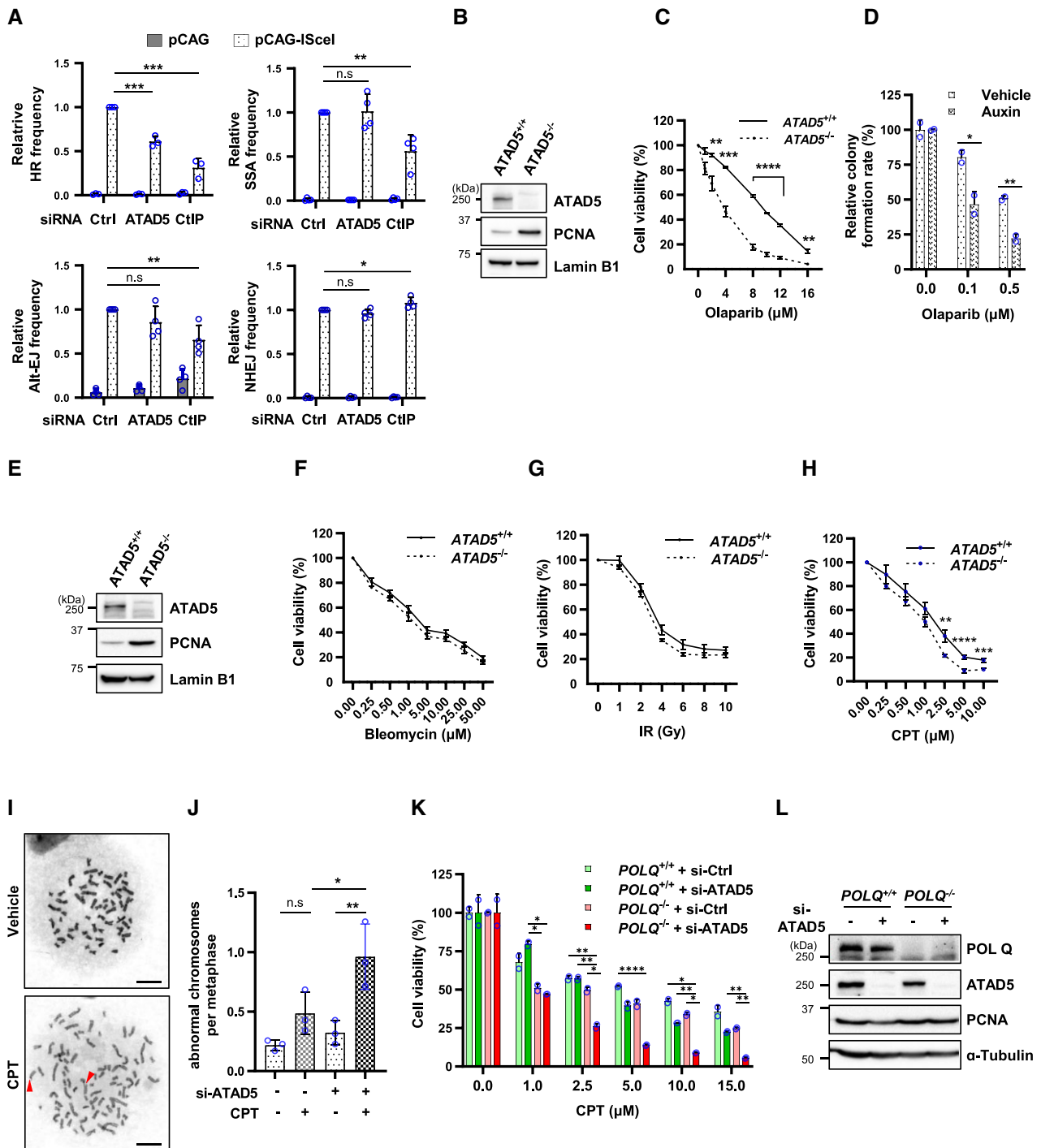
Figure 3. ATAD5-depleted cells are defective for HR and are hypersensitive to camptothecin (CPT). (**A**) DSBR frequency was measured 48 h after transfection with the I-SceI endonuclease using various U2OS reporter cells transfected with *ATAD5* or *CtIP* siRNA. Error bars represent SD (*n* = 3 or 4). Alt-EJ; alternative EJ. (**B**) Chromatin-bound protein extracts were prepared from *ATAD5*+/+ and *ATAD5*−/− HEK293AD cells for immunoblotting. (**C**) *ATAD5*+/+ and *ATAD5*−/− HEK293AD cells were treated with Olaparib for 96 h, allowed to recover for 24 h, and subjected to acute viability assays Error bars represent SD (*n* = 4). (**D**) U2OS-ATAD5^AID cells were pre-treated with auxin for 24 h, then treated with Olaparib for 96 h and subjected to colony forming assay. Auxin was also treated during Olaparib treatment. (**E**) Whole cell extracts were prepared from ATAD5+/+ and ATAD5−/− U2OS cells for immunoblotting. (**F–H**) *ATAD5*+/+ and *ATAD5*−/− U2OS cells were treated with drugs as indicated (for bleomycin, 72 h of treatment and 24 h of recovery; for IR, 5 days of recovery; for CPT, 48 h of treatment) and subjected to acute viability assays. Error bars represent SD (*n* = 3). (I, J) HeLa cells transfected with *ATAD5* siRNA were treated with 1 μM CPT for 1 h and subjected to metaphase spreading. (**I**) A representative image. Arrowheads point to chromosome breaks. Scale bar 10 μm. (**J**) The number of abnormal chromosomes (chromosome break and fragmented chromosome) per cell was counted. Error bars represent SD (*n* = 3). (**K, L**) *POLQ*+/+ and *POLQ*−/− U2OS cells were transfected with *ATAD5* or control siRNA. Cells were treated with CPT 48 h after transfection, and subjected to acute viability assays (K) or immunoblotting with whole cell extracts (L). (K) Error bars represent SD (*n* = 2). Statistical analysis: two-tailed unpaired Student's *t*-test (A, C–D, F–H); one-way ANOVA (J); two-way ANOVA (K).

top left panel), the intensity of RPA2 was increased after IR treatment in wild type cells (top right panel). As reported previously, RPA2 intensity was decreased upon CtIP depletion (7), while this was not the case upon ATAD5 depletion (Supplementary Figure 5C). In line with the flow cytometry-based results, ATAD5 depletion did not affect RPA2 foci induced by IR or CPT (Supplementary Figure 5D–G). Our findings contradict a previous report that showed a reduction of CPT-induced RPA1 foci by ATAD5 depletion (16). One possible explanation for this discrepancy is that the A2780 cells used in the previous study had high endogenous levels of reactive oxygen species (52), which can result in abundant DNA damage, which may lead to a shortage of PCNA available to assist with EXO1-mediated long-range resection (23). In contrast, RFC1 depletion slightly reduced the IR-induced chromatin RPA signal (Supplementary Figure 5H), which can be explained by PCNA increasing long-range end resection by promoting the EXO1 processivity (23). RFC1 depletion consistently reduced the frequency of HR and SSA (Supplementary Figure 5I), which both require long-range resection. RFC1 depletion unexpectedly reduced the frequency of c-NHEJ (Supplementary Figure 5I), suggesting that RFC1 may have an unknown role in this pathway as well. In summary, our results suggest that long-range resection by EXO1 and/or DNA2 occurs normally in ATAD5-depleted cells, cytological methods not being sensitive enough to detect short length resection.

PCNA unloading by ATAD5 is required for MRN-mediated KU removal from DSB ends

Next, we examined the effect of ATAD5 depletion on short-range resection. Removal of KU70/80 heterodimers from tightly bound DSB ends occurs mainly by MRN-CtIP-mediated short-range resection, removal being required for HR (5,6). We hypothesized that PCNA remaining at DSB proximal sites due to ATAD5 depletion may inhibit MRN-mediated short-range resection and subsequent KU removal (Figure 4A). In line with compromised KU removal, we found increased KU80 levels on microirradiated strips in auxin depleted U2OS-ATAD5^{AID} cells (Figure 4B and C).

To corroborate our hypothesis, we assessed KU80 recruitment by counting KU80 foci upon CPT treatment. CPT treatment led to an increased number of KU80 foci (Figure 4D), the number being further increased in either ATAD5- or CtIP-depleted cells (Figure 4E–G). Depletion of both ATAD5 and CtIP did not further increase the number of KU80 foci upon CPT treatment compared to the depletion of either protein alone (Figure 4F), suggesting that two proteins are involved in the same pathway. We found that CtIP levels were increased in ATAD5-depleted cells, whereas ATAD5 levels were increased in CtIP-depleted cells (Figure 4G), suggesting that ATAD5 and CtIP are mutually exclusive in helping to remove KU heterodimers. It is possible that the increase in the number of KU80 foci observed in ATAD5-depleted cells could be due to an overall increase in the number of DSBs. However, this possibility is unlikely because the number of 53BP1 foci, which indicate the presence of DSBs, was similar between control- and ATAD5-depleted cells upon CPT treatment (Figure 4H

and I). ATAD5 specificity was confirmed by complementation upon expressing RNAi resistant wild type ATAD5 (Figure 4J and K). In contrast, consistent with the model that ATAD5 mediated PCNA unloading activity is required for KU80 removal (Figure 4A), expressing the unloading-defective ATAD5 E1173K mutant failed to reduce the number of KU80 foci (Figure 4J). Consistent with PCNA eviction from processed DSBs being defective upon ATAD5 depletion, we found an increased incidence of MRE11 PCNA juxtaposition upon IR in ATAD5-depleted cells not residing in S-phase employing proximity ligation assays (Figure 4L and M). In addition, the reduced HR frequency induced by ATAD5 depletion was significantly restored when KU80 was co-depleted (Figure 4N and O). Partial recovery may be due to incomplete KU80 depletion (Figure 4N and O). Taken together, these results suggest that MRN-mediated resection and ensuing KU removal are inhibited in ATAD5-depleted cells, probably due to PCNA trapped at DSBs.

PCNA loaded on DNA inhibits MRE11/RAD50-mediated resection *in vitro*

We next examined whether DNA bound PCNA can inhibit MRE11-dependent short-range resection. Because of the short length of MRN-mediated resection, it is technically difficult to detect changes in short-range resection using cell-based assays (53). We therefore employed a well-established *in vitro* MRE11/RAD50 (MR) resection assay (40), and combined this with PCNA loading and unloading reactions (12). We generated a 62 bp double-strand DNA (dsDNA) substrate mimicking a nicked DSB. Both ends of the substrate are protected from exonucleolytic degradation, only a centrally located nick with a 3'-OH being accessible to the MR complex and RFC-PCNA (Figure 5A, top left panel). We first confirmed the activity of the purified MR complex on the DNA substrate (Figure 5A, top right panel, and bottom panel) and the suitability of the DNA substrate for PCNA loading by the RFC complex (Figure 5B). We found that adding both the RFC and PCNA before addition of the MR complex decreased MR processing, as observed by the reduced appearance of a biotin-oligonucleotide species, migrating slightly slower than the 16 nt marker (Figure 5C, right-most lane, arrowhead; Figure 5D for quantification). Addition of functional ATAD5-RLC after PCNA loading reaction partly restored the subsequent MR-mediated resection, while adding a PCNA unloading-defective ATAD5(E1173K)-RLC did not (Figure 5E and F). The effect of ATAD5-RLC on MR-mediated resection was minimal, probably due to the concurrent PCNA loading reaction in the reaction tube. Taken together, PCNA loaded on DNA by the RFC complex inhibits MR-mediated end resection, consistent with our results on KU80 removal (Figure 4J and N).

DNA repair synthesis is defective in ATAD5-depleted cells

HR requires the generation of RAD51-coated ssDNA to initiate homology search, and, upon finding a matching sequence, strand invasion to form a displacement loop. Concomitant with RAD51 removal, the invading strand is then extended by DNA synthesis (54,55). Based on long-range
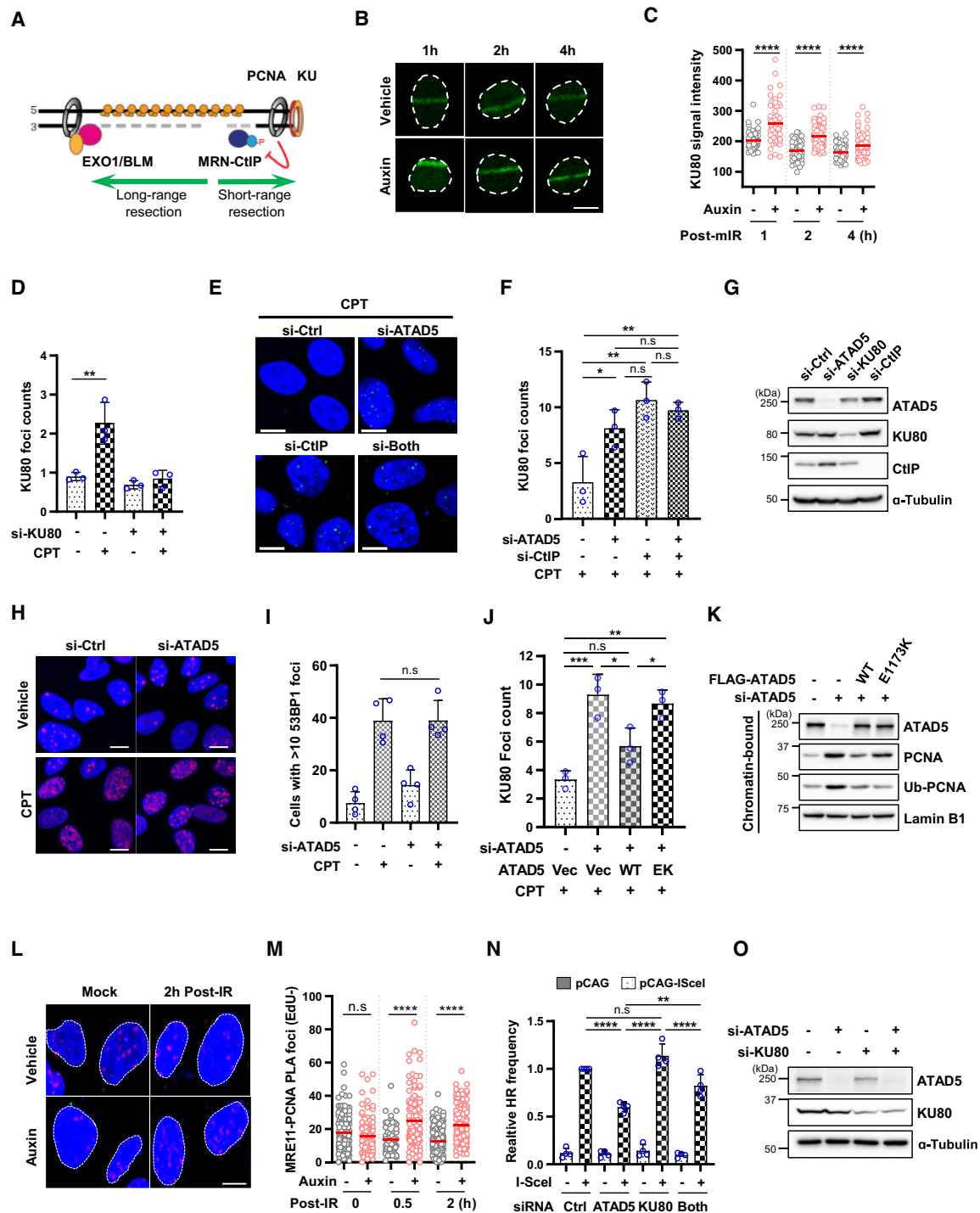
Figure 4. DNA end processing is defective in ATAD5-depleted cells. (**A**) Model for inhibition of MRN-mediated short-range 3′-5′ resection by persisting PCNA. (**B, C**) U2OS-ATAD5^{AID} cells were treated with auxin for 24 h, UV-microirradiated, fixed after the indicated times and stained for KU80. (**B**) Representative images. (**C**) Quantification of KU80 signal intensity on microirradiated strips. (**D–G**) U2OS cells were transfected with siRNAs as indicated. 48 h after transfection, cells were treated with 1 μM CPT for 1 h, and immunostained for KU80 (D–F) or used for generating whole cell extracts for immunoblotting (G). (**E**) Representative images. (D, F) Error bars represent SD ($n = 3$). (**H, I**) U2OS cells were transfected with *ATAD5* siRNA. 48 h after transfection, cells were treated with 1 μM CPT for 1 h, and stained for 53BP1. (**H**) Representative images. (**I**) Error bars represent SD ($n = 4$). (**J, K**) U2OS cells were transfected with a combination of *ATAD5* siRNA and wild type or PCNA unloading-defective E1173K (EK) ATAD5 cDNA as indicated. 48 h after transfection, cells were treated with 1 μM CPT for 1 h, and stained for KU80 (J) or used for preparing chromatin-bound protein extracts prepared for immunoblotting (K). (**L, M**) U2OS-ATAD5^{AID} cells were treated with auxin, labeled with EdU for 30 min, irradiated with 4 Gy of X-ray, and fixed for MRE11-PCNA PLA after the indicated periods of time. (**L**) Representative images. (**M**) Foci was quantified in cells not residing in S phase as determined by the absence of prominent EdU labeling. (**N, O**) U2OS DR-GFP reporter cells were transfected with the I-SceI endonuclease and *ATAD5* or *KU80* siRNA as indicated. 48 h after transfection, HR frequency was measured (N) or whole cell extracts prepared for immunoblotting (O). (N) Error bars represent SD ($n = 3$). Statistical analysis: two-tailed unpaired Student's *t*-test (C, D, M); one-way ANOVA (F, I, J, N). (B, E, H, L) Scale bar 10 μm.
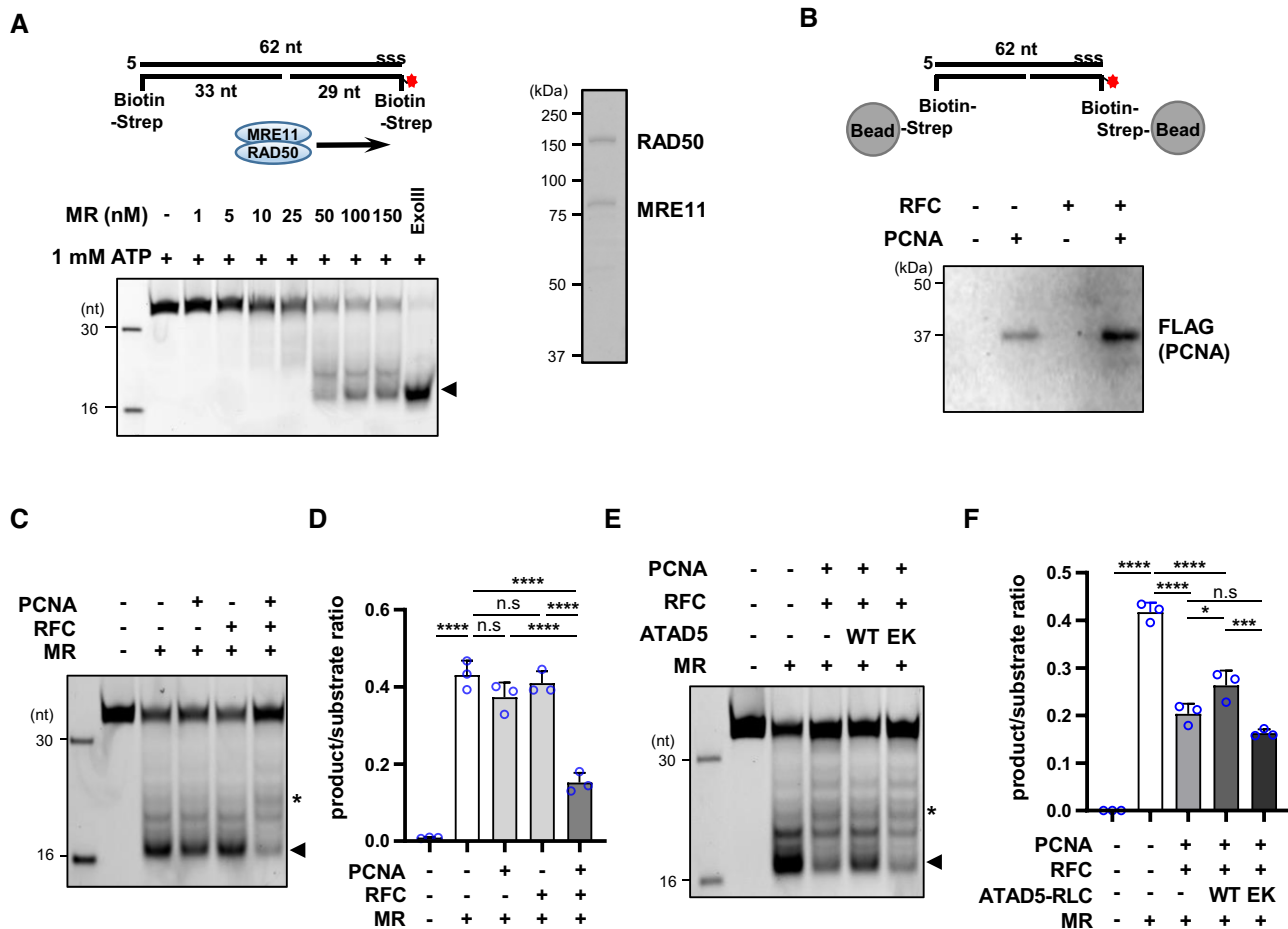
Figure 5. PCNA loaded on DNA blocks MR-mediated resection *in vitro*. (**A**) MR *in vitro* nuclease assay conducted on a substrate that carries a 62-base oligonucleotide (nt) at the top strand, paired to a Cy-5 (red asterisk) and biotin end-labeled 29-base oligonucleotide and a biotin end-labeled 33-base oligonucleotide at the bottom strand. The arrow indicates the direction of the MRE11-RAD50 (MR) exonuclease complex. Both ends of the dsDNA substrate are protected from the exonucleolytic degradation. The 3′ end of bottom strand are protected by streptavidin bound to biotin. The 3′ end of top strand is protected by the incorporation of phosphorothioate bonds (indicated as "sss"). Binding of streptavidin to the 5′ end of the bottom strand is used to mimic KU binding. The assay was conducted with concentration gradient (0–150 nM) of purified human MR (right panel, for Coomassie staining). Nuclease activity was measured by PAGE under denaturing conditions (bottom panel). The arrowhead indicates a resected product. (**B**) A PCNA loading reaction was performed with the same dsDNA substrate, bound to magnetic beads. After washout, proteins on DNA were eluted and subjected to immunoblotting. (**C–F**) *in vitro* MR assay with or without prior RFC-mediated PCNA loading. (E, F) Nuclease assays, on *in vitro* substrate after RFC/PCNA treatment and ensuring incubation with wild type (WT) or PCNA unloading defective ATAD5 (EK, E1173K). (C, E) The Asterisk indicates a partially processed product. (D, F) Error bars represent SD ($n = 3$). Statistical analysis: one-way ANOVA.

resection being intact in ATAD5-depleted cells, while KU80 remains on the site of the initial DSB breakage, we speculated that strand invasion might occur (56), while DNA synthesis might be physically blocked by KU70/80 bound to the initial DSB site (Figure 6A). We therefore measured HR-associated DNA repair synthesis by counting the number of repair foci labeled via the incorporation of the thymidine analog 5-ethynyl-2′-deoxyuridine (EdU) into DNA after IR treatment of G2 cells. We found that the number of EdU foci was reduced upon ATAD5 depletion (Figure 6B, C, For technical detail relating to determining G2 cells, see (Supplementary Figure 6A (19)). We next hypothesized that the blockage of DNA repair synthesis led to an increased steady state of earlier stage HR intermediates stably associated with the RAD51 recombinase, or the RAD54 ATPase needed for RAD51 removal (57,58). Consistent with this hypothesis, we found increased numbers of RAD51

and RAD54 foci in ATAD5-depleted cells (Figure 6D–G), the mean intensity of RAD51 foci being equally increased ((Supplementary Figure 6B). Consistent with KU residence by PCNA trapped at DSBs in ATAD5-depleted cells, KU80 depletion restored the number of IR-induced DNA repair synthesis and RAD51 foci to a level of control (Figure 6H and I). In addition, decreased HR frequency upon ATAD5 depletion was not restored by PCNA unloading-defective ATAD5 (Figure 6J).

Unprocessed DSB ends resulting from ATAD5 depletion are partially repaired by TMEJ

We next aimed to directly test if TMEJ might bypass the HR repair defect associated with the blockage of DNA end resection due to ATAD5 depletion. We adapted the DR-GFP reporter system, where restoration of a functional
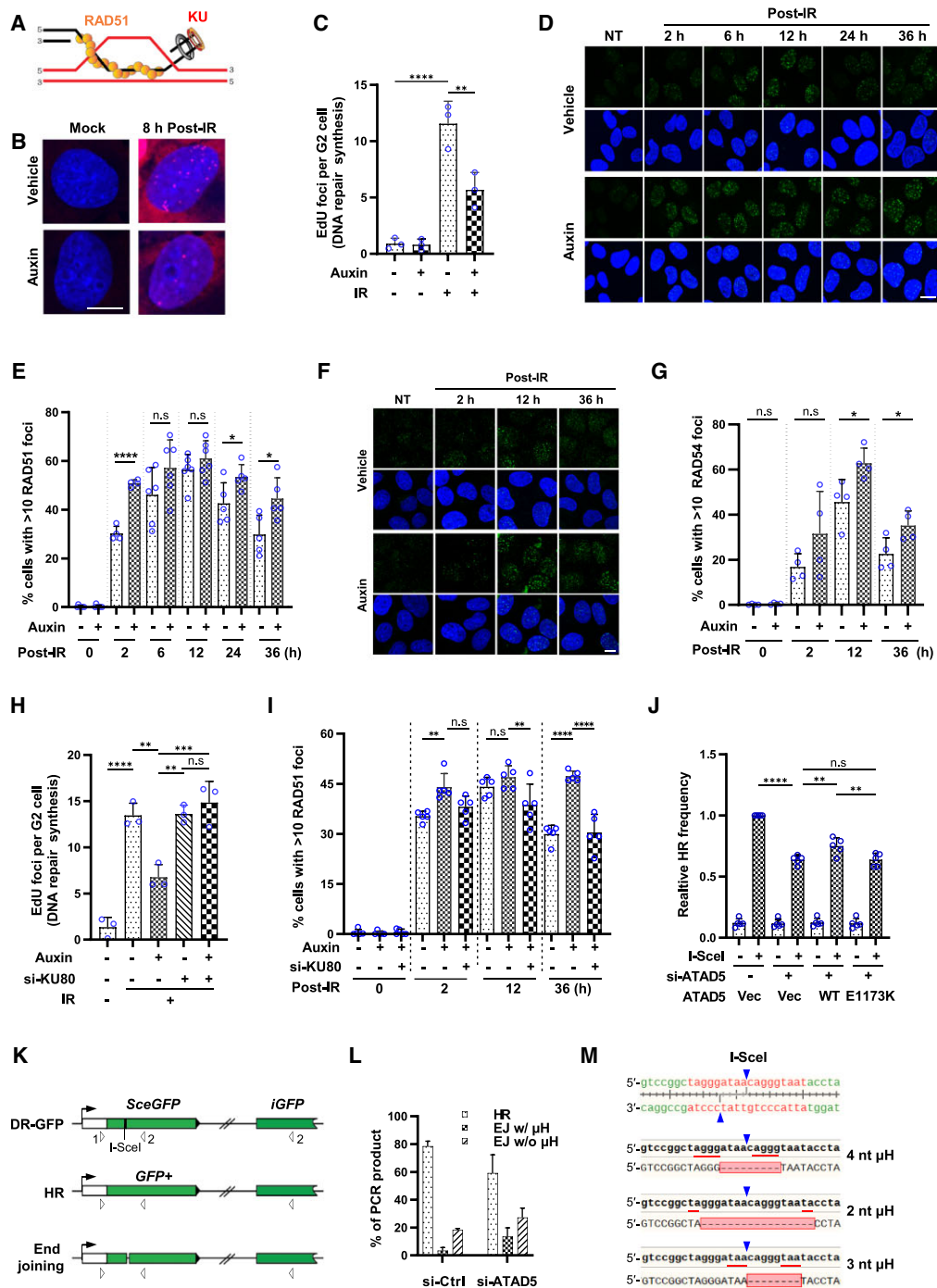
Figure 6. DNA repair synthesis is defective in ATAD5-depleted cells. (**A**) Graphic description for unprocessed DSB ends in ATAD5-depleted cells. (**B, C**) U2OS-ATAD5[AID] cells were treated with auxin, pre-labeled with BrdU, irradiated with X-rays (4 Gy), labeled with EdU for 8 h and fixed. (C) Error bars represent SD ($n = 3$). (**D–G**) U2OS-ATAD5[AID] cells were treated with auxin, irradiated with X-rays (4 Gy), recovered for indicated time and fixed for RAD51 (D, E) or RAD54 immunostaining (F, G). (E, G) Error bars represent SD ($n \geq 4$ [E], $n = 4$ [G]). (**H**) U2OS-ATAD5[AID] cells were transfected with *KU80* siRNA, treated with auxin, pre-labeled with BrdU, irradiated with X-rays (4 Gy), labeled with EdU for 8 h and fixed. Error bars represent SD ($n = 3$). (**I**) U2OS-ATAD5[AID] cells were transfected with *KU80* siRNA, treated with auxin, irradiated with X-rays (4 Gy), recovered for indicated time and fixed for RAD51 immunostaining. Error bars represent SD ($n = 5$). (**J**) HR frequency was measured 48 h after transfection with the I-SceI endonuclease using U2OS DR-GFP reporter cells transfected with a combination of *ATAD5* siRNA and wild type or PCNA unloading-defective E1173K (EK) ATAD5 cDNA. Error bars represent SD ($n = 5$). (**K**) DNA repair substrate (top panel). HR leads to the restoration of GFP by gene conversion (*iGFP*) (middle panel), while end-joining results in small deletions or insertions (bottom panel). The positions of PCR primers are indicated (triangles labeled 1 and 2). (**L**) Amplified repair products of more than 100 were analyzed by sequencing and the proportion of products resulting from HR activity, or end-joining with or without microhomology is displayed ($n = 2$). All HR products, including those with amber mutations, were included for quantification. (**M**) Examples of end-joining products with microhomology (red line) around I-SceI cut sites (blue triangles). Statistical analysis: one-way ANOVA (C, H–J); two-tailed unpaired Student's *t*-test (E, G). (B, D, F) Scale bar 10 μm.

GFP gene is dependent on MRE11 and CtIP (7). To score for the relative incidence of HR and DNA end-joining events, we co-transfected the I-SceI nuclease with texas red cDNA which served as a transfection marker. Fragments corresponding to individual GFP loci were amplified and treated with I-SceI and uncut fragments were cloned and sequenced (Figure 6K). By sequencing ∼100 such fragments derived from mock depleted cells, we found that an average of 78.5% of the fragments were likely repaired by HR because the GFP open reading frame was restored (Figure 6L). Amongst fragments where a functional GFP was not restored and therefore generated by end-joining mechanisms, 15.6% (3.4% in total) showed evidence for microhomology at the breakpoint. In contrast, amongst the ∼100 clones derived from ATAD5 depleted cells, an average of 59.2% resulted from HR, while 33.1% of end-joining-related fragments (13.5% in total) showed microhomology at their breakpoints (Figure 6L and M). Thus, consistent with the weak effect of CPT on the survival of ATAD5 deficient cells (Figure 3H), and the synergistic sensitivity associated with combined POL θ deficiency (Figure 3K), end-joining pathways, particularly TMEJ appears to bypass the HR defects associated with defective end processing in ATAD5-deficient cells.

DISCUSSION

In this study, we show that PCNA is rapidly recruited to laser-induced DSBs in human cell lines. The requirement of RFC1 for the recruitment of PCNA and ATAD5 to DSBs, and the increase of PCNA signal at DSBs upon ATAD5 depletion strongly suggests that PCNA is loaded to DSBs by RFC (Supplementary Figure 6C, iii). Given that PCNA and ATAD5 recruitment to FokI-induced DSBs was not affected by the inhibition of the RAD51 recombinase (Figure 1B and Supplementary Figure 1B) and that recruitment of PCNA to laser microirradiated strips was not affected by BRCA2 depletion (Figure 1E), we propose a role of ATAD5 in removing PCNA, upstream or concomitant with strand invasion. Such a role is in line with the reported association of the budding yeast ATAD5 homolog near DSB sites, independent of the Rad52 mediator protein (18). Based on our genetic analysis combined with *in vitro* experiments, we favor a model where a nick or DNA undergoing initial short-range resection, both catalyzed by MRN-CtIP, are the substrates for PCNA loading (Figure 2 and (Supplementary Figure 6C, ii). Since activation of nick-initiated resection requires CtIP phosphorylation by cyclin-dependent kinases (CDK) (2,3), the CtIP- and RFC-dependent PCNA loading probably occurs only at the S/G2 phases.

PCNA at DSBs has been reported to facilitate EXO1-mediated long-range resection (23). Our results suggest that PCNA loaded at DSBs has the potential to hamper short-range resection and subsequent KU removal unless it is not unloaded by ATAD5-RLC ((Supplementary Figure 6C, v). We favor a model where PCNA molecules loaded at DSBs for increasing EXO1 processivity during long-range resection can become a roadblock hampering MRN-mediated short-range resection. Consistent with this model, PCNA loaded on dsDNA mimicking a nicked DSB inhibits MR-mediated resection *in vitro* (Figure 5), and impeding short-

range resection by ATAD5 depletion leads to an increased proximity of MRE11 and PCNA as measured by proximity ligation assays. According to our model, impeding short-range end resection also attenuates the removal of KU70/80 bound to the original DSB end, in line with our cytological results in ATAD5 deficient cells. Our results indicate that long-range resection proceeds normally in ATAD5 deficient cells (Supplementary Figure 5), and that foci possibly indicative of invading ssDNA-RAD51 filaments appear to form (Figure 6D and (Supplementary Figure 6C, b, vi). It is conceivable that strand invasion occurs despite the 3′ end of the invading strand being double-stranded and being bound to KU70/80, both due to the failure to complete end resection. The terminal 3′-OH of the invading strand being blocked would inhibit DNA repair synthesis needed for the completion of HR, in line with the reduced EdU incorporation, indicative of DNA repair synthesis, observed upon IR treatment of ATAD5 deficient cells (Figure 6B and C). There is direct evidence that strand invasion by ssDNA-RAD51 can be nucleated from internal sites, not requiring a free terminal 3′-OH (56), in line with a single ssDNA-RAD51 filament being able to invade multiple donor DNA sites simultaneously in yeast cells (59). All in all, we speculate that the ssDNA-RAD51 filaments in ATAD5 deficient cells engage in strand invasion despite KU70/80 being terminally bound to the invading strand ((Supplementary Figure 6C, b, vii).

A previous report also showed that PCNA rapidly accumulated at laser-induced DNA damage in human cells, but, in this study, the association was independent of RFC1 (22), which is different from our results (Figure 1E). PCNA may be recruited to laser-induced DNA damage which include DSB, SSB and other forms of DNA damage, and being loaded by repair proteins such as XRCC1 (34). In addition, differences in irradiation sources or doses can also affect the way PCNA is recruited, resulting in differential RFC dependencies (22). At DSBs, pathways partially redundant with PCNA loading by RFC may exist. PCNA might also be loaded by alternative clamp loaders such as CTF18-RLC (12,60), or via interacting with repair proteins. Our data is consistent with such redundancy as ATAD5 localization at FokI-induced DSBs is only reduced by half upon RFC1 depletion (Figure 1B).

Given the dual role of MRN in nick generation and subsequent exonucleolytic resection, it is not clear if PCNA is loaded at the nick, or if loading requires initial exonucleolytic resection, and if PCNA is loaded between MRN and the DSB end, or to the 5′ of the resecting MRN complex. MRN changes its conformation between open and closed upon ATP binding and hydrolysis, and each conformation affects the endo- or exonuclease activity of MRE11 differently (53). In addition, structural studies of MR-like complexes in bacteria suggested that MRE11 takes up a different position relative to RAD50 at DSBs depending on whether it generates an endonucleolytic nick or resects DNA (61). These suggest that nick generation and subsequent resection might be carried out not by a single MRN complex, the requirement of two or more complexes with different conformations tailored for endonucleolytic attack, or end resection being more likely. It will require further investigation to decide if nick generation and

short-range resection are catalyzed by distinct complexes and if PCNA may be loaded between the nick generation and end resection.

ATAD5-depleted cells are sensitive to drugs forming protein-DNA adducts at the DSB (Figure 3), MRN-CtIP being required for adduct removal. We propose that defective end processing and the failure to form a free 3′-OH end due to PCNA trapped at nicked DSBs is the underlying mechanism for HR defects and the drug sensitivity in ATAD5-deficient cells. The TMEJ pathway has the potential to repair resected DSBs not processed by HR. A backup role of TMEJ is also evident in BRCA1 or BRCA2 deficient cells (62), these cells becoming critically dependent on TMEJ for survival (63,64). Consistent with this idea, we observed a high level of end-joining products with microhomology using the DR-GFP reporter system in ATAD5-depleted cells (Figure 6L). Furthermore, the synergetic CPT sensitivity conferred by the co-depletion of ATAD5 and POLθ supports TMEJ as an alternative mechanism for repairing DSBs with unprocessed ends (Figure 3K).

In EJ2-GFP DNA, which detects TMEJ, the microhomology domain is just adjacent to the I-SceI-induced DSB ends and is therefore likely to be covered by KU heterodimers (Supplementary Figure 2C). In addition, the end-joining-related fragments of DR-GFP DNA showed microhomology at the breakpoints (Figure 6M), which could be covered by KU heterodimers. We maintain that the KU heterodimer-mediated inhibition upon ATAD5 depletion will not affect TMEJ frequency for EJ2-GFP DNA and the use of TMEJ for unprocessed DSB ends of DR-GFP DNA, at least in the S/G2 phase, because TMEJ is already blocked by HR proteins such as BRCA2 and RPA bound to long resected DNA in this cell cycle phase (62,65). HR is inhibited in mitosis by CDK-dependent BRCA2 phosphorylation and following disruption of the BRCA2–RAD51 interaction (66). Although, according to the same study, HR is restored by suppression of CDK activities mediated by DNA damage checkpoint activation, this is unlikely to apply to the I-SceI-based system, as it was reported that an I-SceI-induced break at one locus did to not cause checkpoint activation (67). A recent research has shown that ssDNA-RAD51 filaments do not inhibit the DNA polymerase activity of POLθ (62). The same report also showed that TMEJ-mediated repair of the long resected DNA takes place during mitosis, although it was studied in cells that were deficient in BRCA2. Taken together, TMEJ may act primarily in the mitosis. If this is the case, what is missing from our study is whether and how the KU heterodimers bound to DSB ends are ultimately removed for TMEJ to occur in ATAD5-depleted cells. We speculate that a phosphorylation- or ubiquitination-mediated dissociation of the KU heterodimer from the DNA ends (68,69), just at the time when TMEJ is active, may be involved. Although this requires further analysis, our results strongly suggest that intact long-range resection and usage of TMEJ for unprocessed ends may occur simultaneously.

Unlike TMEJ, c-NHEJ does not appear to be used to repair unprocessed DSB ends of the DR-GFP reporter in ATAD5-depleted cells (Figure 6L). In addition, the repair frequency of the EJ5-GFP reporter, which detects c-NHEJ (Supplementary Figure 2D), was not altered by ATAD5 depletion (Figure 3A). This suggests that in both reporter DNAs broken in the S/G2 phase, the remaining KU heterodimers at DSB ends due to ATAD5 depletion did not lead to an increase in c-NHEJ. We speculate that the DSBR pathways for fixing either reporter DNA are already committed to ones accompanying end resection following I-SceI expression in the S/G2 phase. Therefore, although the DSB ends of both reporter DNAs remain bound to KU heterodimers, the repair pathway may not be redirected to c-NHEJ.

In summary, we propose that PCNA loading and unloading are tightly regulated when DSB breaks are bidirectionally processed during DNA end resection. PCNA unloading by ATAD5-RLC is required to facilitate the completion of short-range resection to ensure a free 3′-OH group needed to prime DNA synthesis to extend the invading strand. We speculate that the role of ATAD5 in DSB repair, in conjunction with its role in mediating DNA replication fork stability and the prevention and resolution of R-loops (30,33), provides a molecular mechanism that contributes to the tumor-suppressive function of ATAD5.

DATA AVAILABILITY

The data underlying this article are available in the article and in its online supplementary material.

SUPPLEMENTARY DATA

Supplementary Data are available at NAR Online.

REFERENCES

1. Ceccaldi,R., Rondinelli,B. and D'Andrea,A.D. (2016) Repair pathway choices and consequences at the double-strand break. *Trends Cell Biol.*, **26**, 52–64.
2. Ferretti,L.P., Lafranchi,L. and Sartori,A.A. (2013) Controlling DNA-end resection: a new task for CDKs. *Front Genet.*, **4**, 99.
3. Shibata,A. (2017) Regulation of repair pathway choice at two-ended DNA double-strand breaks. *Mutat. Res.*, **803-805**, 51–55.
4. Symington,L.S. (2016) Mechanism and regulation of DNA end resection in eukaryotes. *Crit. Rev. Biochem. Mol. Biol.*, **51**, 195–212.
5. Langerak,P., Mejia-Ramirez,E., Limbo,O. and Russell,P. (2011) Release of Ku and MRN from DNA ends by Mre11 nuclease activity and Ctp1 is required for homologous recombination repair of double-strand breaks. *PLoS Genet.*, **7**, e1002271.

6. Chanut,P., Britton,S., Coates,J., Jackson,S.P. and Calsou,P. (2016) Coordinated nuclease activities counteract Ku at single-ended DNA double-strand breaks. *Nat. Commun.*, **7**, 12889.

7. Sartori,A.A., Lukas,C., Coates,J., Mistrik,M., Fu,S., Bartek,J., Baer,R., Lukas,J. and Jackson,S.P. (2007) Human CtIP promotes DNA end resection. *Nature*, **450**, 509–514.

8. Boehm,E.M., Gildenberg,M.S. and Washington,M.T. (2016) The Many Roles of PCNA in Eukaryotic DNA Replication. *Enzymes*, **39**, 231–254.

9. Moldovan,G.L., Pfander,B. and Jentsch,S. (2007) PCNA, the maestro of the replication fork. *Cell*, **129**, 665–679.

10. Majka,J. and Burgers,P.M. (2004) The PCNA-RFC families of DNA clamps and clamp loaders. *Prog. Nucleic Acid Res. Mol. Biol.*, **78**, 227–260.

11. Yao,N.Y. and O'Donnell,M. (2012) The RFC clamp loader: structure and function. *Subcell. Biochem.*, **62**, 259–279.

12. Kang,M.S., Ryu,E., Lee,S.W., Park,J., Ha,N.Y., Ra,J.S., Kim,Y.J., Kim,J., Abdel-Rahman,M., Park,S.H. *et al.* (2019) Regulation of PCNA cycling on replicating DNA by RFC and RFC-like complexes. *Nat. Commun.*, **10**, 2420.

13. Lee,K.Y., Fu,H., Aladjem,M.I. and Myung,K. (2013) ATAD5 regulates the lifespan of DNA replication factories by modulating PCNA level on the chromatin. *J. Cell Biol.*, **200**, 31–44.

14. Kubota,T., Nishimura,K., Kanemaki,M.T. and Donaldson,A.D. (2013) The Elg1 replication factor C-like complex functions in PCNA unloading during DNA replication. *Mol. Cell*, **50**, 273–280.

15. Herr,P., Lundin,C., Evers,B., Ebner,D., Bauerschmidt,C., Kingham,G., Palmai-Pallag,T., Mortusewicz,O., Frings,O., Sonnhammer,E. *et al.* (2015) A genome-wide IR-induced RAD51 foci RNAi screen identifies CDC73 involved in chromatin remodeling for DNA repair. *Cell Discov.*, **1**, 15034.

16. Giovannini,S., Weller,M.C., Hanzlikova,H., Shiota,T., Takeda,S. and Jiricny,J. (2020) ATAD5 deficiency alters DNA damage metabolism and sensitizes cells to PARP inhibition. *Nucleic Acids Res.*, **48**, 4928–4939.

17. Sikdar,N., Banerjee,S., Lee,K.Y., Wincovitch,S., Pak,E., Nakanishi,K., Jasin,M., Dutra,A. and Myung,K. (2009) DNA damage responses by human ELG1 in S phase are important to maintain genomic integrity. *Cell Cycle*, **8**, 3199–3207.

18. Ogiwara,H., Ui,A., Enomoto,T. and Seki,M. (2007) Role of Elg1 protein in double strand break repair. *Nucleic Acids Res.*, **35**, 353–362.

19. Juhasz,S., Elbakry,A., Mathes,A. and Lobrich,M. (2018) ATRX promotes DNA repair synthesis and sister chromatid exchange during homologous recombination. *Mol. Cell*, **71**, 11–24.

20. Elbakry,A., Juhasz,S., Chan,K.C. and Lobrich,M. (2021) ATRX and RECQ5 define distinct homologous recombination subpathways. *Proc. Natl. Acad. Sci. U.S.A.*, **118**, e2010370118.

21. Li,X., Stith,C.M., Burgers,P.M. and Heyer,W.D. (2009) PCNA is required for initiation of recombination-associated DNA synthesis by DNA polymerase delta. *Mol. Cell*, **36**, 704–713.

22. Hashiguchi,K., Matsumoto,Y. and Yasui,A. (2007) Recruitment of DNA repair synthesis machinery to sites of DNA damage/repair in living human cells. *Nucleic Acids Res.*, **35**, 2913–2923.

23. Chen,X., Paudyal,S.C., Chin,R.I. and You,Z. (2013) PCNA promotes processive DNA end resection by Exo1. *Nucleic Acids Res.*, **41**, 9325–9338.

24. Lee,K.Y. and Park,S.H. (2020) Eukaryotic clamp loaders and unloaders in the maintenance of genome stability. *Exp. Mol. Med.* **52**, 1948–1958.

25. Bell,D.W., Sikdar,N., Lee,K.Y., Price,J.C., Chatterjee,R., Park,H.D., Fox,J., Ishiai,M., Rudd,M.L., Pollock,L.M. *et al.* (2011) Predisposition to cancer caused by genetic and functional defects of mammalian Atad5. *PLos Genet.*, **7**, e1002245.

26. Maleva Kostovska,I., Wang,J., Bogdanova,N., Schurmann,P., Bhuju,S., Geffers,R., Durst,M., Liebrich,C., Klapdor,R., Christiansen,H. *et al.* (2016) Rare ATAD5 missense variants in breast and ovarian cancer patients. *Cancer Lett.*, **376**, 173–177.

27. Kuchenbaecker,K.B., Ramus,S.J., Tyrer,J., Lee,A., Shen,H.C., Beesley,J., Lawrenson,K., McGuffog,L., Healey,S., Lee,J.M. *et al.* (2015) Identification of six new susceptibility loci for invasive epithelial ovarian cancer. *Nat. Genet.*, **47**, 164–171.

28. Johnson,C., Gali,V.K., Takahashi,T.S. and Kubota,T. (2016) PCNA retention on DNA into G2/M phase causes genome instability in cells lacking Elg1. *Cell Rep.*, **16**, 684–695.

29. Shemesh,K., Sebesta,M., Pacesa,M., Sau,S., Bronstein,A., Parnas,O., Liefshitz,B., Venclovas,C., Krejci,L. and Kupiec,M. (2017) A structure-function analysis of the yeast Elg1 protein reveals the importance of PCNA unloading in genome stability maintenance. *Nucleic Acids Res.*, **45**, 3189–3203.

30. Park,S.H., Kang,N., Song,E., Wie,M., Lee,E.A., Hwang,S., Lee,D., Ra,J.S., Park,I.B., Park,J. *et al.* (2019) ATAD5 promotes replication restart by regulating RAD51 and PCNA in response to replication stress. *Nat. Commun.*, **10**, 5718.

31. Shiomi,Y. and Nishitani,H. (2013) Alternative replication factor C protein, Elg1, maintains chromosome stability by regulating PCNA levels on chromatin. *Genes Cells*, **18**, 946–959.

32. Park,S.H., Kim,Y., Ra,J.S., Wie,M.W., Kang,M.S., Kang,S., Myung,K. and Lee,K.Y. (2021) Timely termination of repair DNA synthesis by ATAD5 is important in oxidative DNA damage-induced single-strand break repair. *Nucleic Acids Res.*, **49**, 11746–11764.

33. Kim,S., Kang,N., Park,S.H., Wells,J., Hwang,T., Ryu,E., Kim,B.G., Hwang,S., Kim,S.J., Kang,S. *et al.* (2020) ATAD5 restricts R-loop formation through PCNA unloading and RNA helicase maintenance at the replication fork. *Nucleic Acids Res.*, **48**, 7218–7238.

34. Hwang,T., Reh,S., Dunbayev,Y., Zhong,Y., Takata,Y., Shen,J., McBride,K.M., Murnane,J.P., Bhak,J., Lee,S. *et al.* (2020) Defining the mutation signatures of DNA polymerase theta in cancer genomes. *NAR Cancer*, **2**, zcaa017.

35. Kim,S.J., Wie,M., Park,S.H., Kim,T.M., Park,J.H., Kim,S., Myung,K. and Lee,K.Y. (2020) ATAD5 suppresses centrosome over-duplication by regulating UAF1 and ID1. *Cell Cycle*, **19**, 1952–1968.

36. Lee,K.Y., Yang,K., Cohn,M.A., Sikdar,N., D'Andrea,A.D. and Myung,K. (2010) Human ELG1 regulates the level of ubiquitinated proliferating cell nuclear antigen (PCNA) through Its interactions with PCNA and USP1. *J. Biol. Chem.*, **285**, 10362–10369.

37. Britton,S., Coates,J. and Jackson,S.P. (2013) A new method for high-resolution imaging of Ku foci to decipher mechanisms of DNA double-strand break repair. *J. Cell Biol.*, **202**, 579–595.

38. Gunn,A. and Stark,J.M. (2012) I-SceI-based assays to examine distinct repair outcomes of mammalian chromosomal double strand breaks. *Methods Mol. Biol.*, **920**, 379–391.

39. Shibata,A., Conrad,S., Birraux,J., Geuting,V., Barton,O., Ismail,A., Kakarougkas,A., Meek,K., Taucher-Scholz,G., Lobrich,M. *et al.* (2011) Factors determining DNA double-strand break repair pathway choice in G2 phase. *EMBO J.*, **30**, 1079–1092.

40. Deshpande,R.A., Lee,J.H., Arora,S. and Paull,T.T. (2016) Nbs1 converts the human Mre11/Rad50 nuclease complex into an endo/exonuclease machine specific for protein-DNA adducts. *Mol. Cell*, **64**, 593–606.

41. Tang,J., Cho,N.W., Cui,G., Manion,E.M., Shanbhag,N.M., Botuyan,M.V., Mer,G. and Greenberg,R.A. (2013) Acetylation limits 53BP1 association with damaged chromatin to promote homologous recombination. *Nat. Struct. Mol. Biol.*, **20**, 317–325.

42. Huang,F., Motlekar,N.A., Burgwin,C.M., Napper,A.D., Diamond,S.L. and Mazin,A.V. (2011) Identification of specific inhibitors of human RAD51 recombinase using high-throughput screening. *ACS Chem. Biol.*, **6**, 628–635.

43. Kang,M.S., Kim,J., Ryu,E., Ha,N.Y., Hwang,S., Kim,B.G., Ra,J.S., Kim,Y.J., Hwang,J.M., Myung,K. *et al.* (2019) PCNA unloading is negatively regulated by BET proteins. *Cell Rep.*, **29**, 4632–4645.

44. Yun,M.H. and Hiom,K. (2009) CtIP-BRCA1 modulates the choice of DNA double-strand-break repair pathway throughout the cell cycle. *Nature*, **459**, 460–463.

45. Bajrami,I., Frankum,J.R., Konde,A., Miller,R.E., Rehman,F.L., Brough,R., Campbell,J., Sims,D., Rafiq,R., Hooper,S. *et al.* (2014) Genome-wide profiling of genetic synthetic lethality identifies CDK12 as a novel determinant of PARP1/2 inhibitor sensitivity. *Cancer Res.*, **74**, 287–297.

46. Farmer,H., McCabe,N., Lord,C.J., Tutt,A.N., Johnson,D.A., Richardson,T.B., Santarosa,M., Dillon,K.J., Hickson,I., Knights,C. *et al.* (2005) Targeting the DNA repair defect in BRCA mutant cells as a therapeutic strategy. *Nature*, **434**, 917–921.

47. Bryant,H.E., Schultz,N., Thomas,H.D., Parker,K.M., Flower,D., Lopez,E., Kyle,S., Meuth,M., Curtin,N.J. and Helleday,T. (2005) Specific killing of BRCA2-deficient tumours with inhibitors of poly(ADP-ribose) polymerase. *Nature*, **434**, 913–917.

48. Olivieri,M., Cho,T., Alvarez-Quilon,A., Li,K., Schellenberg,M.J., Zimmermann,M., Hustedt,N., Rossi,S.E., Adam,S., Melo,H. *et al.* (2020) A genetic map of the response to DNA damage in human cells. *Cell*, **182**, 481–496.

49. Pommier,Y. (2006) Topoisomerase I inhibitors: camptothecins and beyond. *Nat. Rev. Cancer*, **6**, 789–802.

50. Sau,S., Liefshitz,B. and Kupiec,M. (2019) The yeast PCNA unloader Elg1 RFC-like complex plays a role in eliciting the DNA damage checkpoint. *Mbio*, **10**, e01159-19.

51. Blackford,A.N. and Jackson,S.P. (2017) ATM, ATR, and DNA-PK: the Trinity at the Heart of the DNA Damage Response. *Mol. Cell*, **66**, 801–817.

52. Xia,C., Meng,Q., Liu,L.Z., Rojanasakul,Y., Wang,X.R. and Jiang,B.H. (2007) Reactive oxygen species regulate angiogenesis and tumor growth through vascular endothelial growth factor. *Cancer Res.*, **67**, 10823–10830.

53. Reginato,G. and Cejka,P. (2020) The MRE11 complex: a versatile toolkit for the repair of broken DNA. *DNA Repair (Amst.)*, **91-92**, 102869.

54. Kowalczykowski,S.C. (2015) An overview of the molecular mechanisms of recombinational DNA repair. *Cold Spring Harb. Perspect. Biol.*, **7**, a016410.

55. Heyer,W.D., Ehmsen,K.T. and Liu,J. (2010) Regulation of homologous recombination in eukaryotes. *Annu. Rev. Genet.*, **44**, 113–139.

56. De Vlaminck,I., van Loenhout,M.T., Zweifel,L., den Blanken,J., Hooning,K., Hage,S., Kerssemakers,J. and Dekker,C. (2012) Mechanism of homology recognition in DNA recombination from dual-molecule experiments. *Mol. Cell*, **46**, 616–624.

57. Li,X. and Heyer,W.D. (2009) RAD54 controls access to the invading 3'-OH end after RAD51-mediated DNA strand invasion in homologous recombination in Saccharomyces cerevisiae. *Nucleic Acids Res.*, **37**, 638–646.

58. Crickard,J.B., Moevus,C.J., Kwon,Y., Sung,P. and Greene,E.C. (2020) Rad54 drives ATP hydrolysis-dependent DNA sequence alignment during homologous recombination. *Cell*, **181**, 1380–1394.

59. Piazza,A., Wright,W.D. and Heyer,W.D. (2017) Multi-invasions are recombination byproducts that induce chromosomal rearrangements. *Cell*, **170**, 760–773.

60. Bylund,G.O. and Burgers,P.M. (2005) Replication protein A-directed unloading of PCNA by the Ctf18 cohesion establishment complex. *Mol. Cell. Biol.*, **25**, 5445–5455.

61. Kashammer,L., Saathoff,J.H., Lammens,K., Gut,F., Bartho,J., Alt,A., Kessler,B. and Hopfner,K.P. (2019) Mechanism of DNA end sensing and processing by the Mre11-Rad50 complex. *Mol. Cell*, **76**, 382–394.

62. Llorens-Agost,M., Ensminger,M., Le,H.P., Gawai,A., Liu,J., Cruz-Garcia,A., Bhetawal,S., Wood,R.D., Heyer,W.D. and Lobrich,M. (2021) POLtheta-mediated end joining is restricted by RAD52 and BRCA2 until the onset of mitosis. *Nat. Cell Biol.*, **23**, 1095–1104.

63. Mateos-Gomez,P.A., Gong,F., Nair,N., Miller,K.M., Lazzerini-Denchi,E. and Sfeir,A. (2015) Mammalian polymerase theta promotes alternative NHEJ and suppresses recombination. *Nature*, **518**, 254–257.

64. Ceccaldi,R., Liu,J.C., Amunugama,R., Hajdu,I., Primack,B., Petalcorin,M.I., O'Connor,K.W., Konstantinopoulos,P.A., Elledge,S.J., Boulton,S.J. *et al.* (2015) Homologous-recombination-deficient tumours are dependent on Poltheta-mediated repair. *Nature*, **518**, 258–262.

65. Mateos-Gomez,P.A., Kent,T., Deng,S.K., McDevitt,S., Kashkina,E., Hoang,T.M., Pomerantz,R.T. and Sfeir,A. (2017) The helicase domain of Poltheta counteracts RPA to promote alt-NHEJ. *Nat. Struct. Mol. Biol.*, **24**, 1116–1123.

66. Esashi,F., Christ,N., Gannon,J., Liu,Y., Hunt,T., Jasin,M. and West,S.C. (2005) CDK-dependent phosphorylation of BRCA2 as a regulatory mechanism for recombinational repair. *Nature*, **434**, 598–604.

67. Dodson,H. and Morrison,C.G. (2009) Increased sister chromatid cohesion and DNA damage response factor localization at an enzyme-induced DNA double-strand break in vertebrate cells. *Nucleic Acids Res.*, **37**, 6054–6063.

68. Postow,L., Ghenoiu,C., Woo,E.M., Krutchinsky,A.N., Chait,B.T. and Funabiki,H. (2008) Ku80 removal from DNA through double strand break-induced ubiquitylation. *J. Cell Biol.*, **182**, 467–479.

69. Lee,K.J., Saha,J., Sun,J., Fattah,K.R., Wang,S.C., Jakob,B., Chi,L., Wang,S.Y., Taucher-Scholz,G., Davis,A.J. *et al.* (2016) Phosphorylation of Ku dictates DNA double-strand break (DSB) repair pathway choice in S phase. *Nucleic Acids Res.*, **44**, 1732–1745.